

We are IntechOpen, the world's leading publisher of Open Access books Built by scientists, for scientists

6,900

Open access books available

186,000

International authors and editors

200M

Downloads

Our authors are among the

154

Countries delivered to

TOP 1%

most cited scientists

12.2%

Contributors from top 500 universities



WEB OF SCIENCE™

Selection of our books indexed in the Book Citation Index
in Web of Science™ Core Collection (BKCI)

Interested in publishing with us?
Contact book.department@intechopen.com

Numbers displayed above are based on latest data collected.
For more information visit www.intechopen.com



Acoustic Waves in Layered Media - From Theory to Seismic Applications

Alexey Stovas¹ and Yury Roganov²

¹NTNU, Trondheim,

²USGPI, Kiev,

¹Norway

²Ukraine

1. Introduction

Acoustic wave propagation in layered media is very important topic for many practical applications including medicine, optics and applied geophysics. The key parameter controlling all effects in layered media is the scaling factor given by the ratio between the wavelength and the layer thickness. Existing theory mostly covers the solutions derived for the low-frequency and high-frequency limits. In the first limit, when the wavelength is much larger than the layer thickness, the layered medium is substituted by an effective medium with the properties given by special technique called the Backus averaging. In the second limit, when the wavelength is much smaller than the layer thickness, we can use the ray theory to compute both reflection and transmission responses.

In practice, the wavelength could be comparable with the layer thickness, and application of both frequency limits is no longer valid. In this chapter, we will mainly focus on the frequency-dependent effects for acoustic waves propagating through the layered media.

We show that there are distinct periodically repeated patterns consisted of the pass- and stop-bands of very complicated configuration defined in frequency-slowness or frequency-group angle domain that control the reflection and transmission responses. The edges between the pass- and stop-bands result in the caustics in the group domain. The quasi-shear waves in a homogeneous transversely isotropic medium could also results in the high-frequency caustics, but for the layered media, all wave modes can result in frequency-dependent caustics. The caustics computed for a specific frequency differ from those observed at the low- and high-frequency limits. From physics point of view, the pass-bands correspond to the effective medium, while the stop-bands correspond to the resonant medium. We distinguish between the effects of scattering and intrinsic attenuation in layered media. The propagation of acoustic waves in a layered medium results in the energy loss due to scattering effect. The intrinsic attenuation is an additional effect which plays very important role in seismic data inversion. We provide the theoretical and numerical study to compare both effects for a periodically layered medium. We also investigate the complex frequency roots of the reflection/transmission responses. We also derive the phase velocity approximations in a layered medium. As the trial model for layered medium, we widely use the periodically layered medium with the limited number of parameters. The propagation of acoustic waves through a periodic layered medium is analyzed by an eigenvalue

decomposition of the propagator matrix. This reveals how the velocity and attenuation of the layered medium vary as function of the periodic structure, material parameters and frequency. We show that there is one more parameter controlling the wave propagation apart of the wavelength to layer thickness ratio that is the acoustic contrast between the layers. Multiple scattering in finely layered sediments is important in stratigraphic interpretation in seismic, matching of well log-data with seismic data and seismic modelling. Two methods have been used to treat this problem in seismic applications: the O'Doherty-Anstey approximation and Backus averaging. The O'Doherty-Anstey approximation describes the stratigraphic filtering effects, while the Backus averaging defines the elastic properties for an effective medium from the stack of the layers.

Using numerical examples, we show that there is a transition zone between the effective medium (low-frequency limit) and the time-average medium (high-frequency limit) and that the width of this zone depends on the strength of the reflection coefficient series. Assuming that a turbidite reservoir can be approximated by a stack of thin shale-sand layers we use standard AVO-attributes to estimate net-to-gross and oil saturation. Necessary input is Gassmann rock physics properties for sand and shale as well as the fluid properties for hydrocarbons. Required seismic input is AVO intercept and gradient. The method is based upon thin layer reflectivity modeling. It is shown that random variability in thickness and seismic properties of the thin sand and shale layers does not change the AVO attributes at top and base of the turbidite reservoir sequence significantly. The method is tested on seismic data from offshore Brazil, and the results show reasonable agreement between estimated and observed net-to-gross and oil saturation. The methodology can be further developed for estimating changes in pay thickness from time lapse seismic data. We propose the method of computation seismic AVO attributes (intercept and gradient) from ultra-thin geological model based on the SBED modelling software. The SBED software is based on manipulating sine-functions, creating surfaces representing incremental sedimentation. Displacement of the surfaces creates a three dimensional image mimicking bedform migration, and depositional environments as diverse as tidal channels and mass flows can be accurately recreated. The resulting modelled deposit volume may be populated with petrophysical information, creating intrinsic properties such as porosity and permeability (both vertical and horizontal). The Backus averaging technique is used for up-scaling within the centimetre scale (the intrinsic net-to-gross value controls the acoustic properties of the ultra-thin layers). It results in pseudo-log data including the intrinsic anisotropy parameters. The synthetic seismic modelling is given by the matrix propagator method allows us to take into account all pure mode multiples, and resulting AVO attributes become frequency dependent. Within this ultra-thin model we can test different fluid saturation scenarios and quantify the likelihood of possible composite analogues. This modelling can also be used for inversion of real seismic data into net-to-gross and fluid saturation for ultra-thin reservoirs.

There are many other issues related to wave propagation in layered media we do not discuss in this chapter. For further reading we suggest several books (Aki&Richards, 1980; Brekhovskih, 1960; Kennett, 1983; Tsvankin, 1995) that cover the problems we did not touch here.

2. System of differential equations

To describe the dynamic of the wave propagation in an elastic medium, it is common to use the Hook's law that defines the linear relation between the stress tensor τ_{ij} and the strains tensor e_{pq} ,

$$\tau_{ij} = c_{ijpq} e_{pq}, \quad (1)$$

where $e_{pq} = \frac{1}{2} \left(\frac{\partial u_p}{\partial x_q} + \frac{\partial u_q}{\partial x_p} \right)$ and c_{ijpq} is the stiffness tensor. If there are no volume forces within the medium, we can write the moment equation in the following way (Aki and Richards, 1980)

$$\rho \frac{\partial^2 u_i}{\partial t^2} = \frac{\partial \tau_{ij}}{\partial x_j}. \quad (2)$$

In equation (1) and (2), it is assumed that the summation is performed over the repeatable indices. Since the tensor c_{ijpq} is symmetrical with respect to index changing $(ij) \leftrightarrow (pq)$, $i \leftrightarrow j$, $p \leftrightarrow q$, the relation (1) can be written as

$$\tau_{ij} = c_{ijpq} \frac{\partial u_p}{\partial x_q}. \quad (3)$$

If we denote $v_i = \frac{\partial u_i}{\partial t}$ as the velocity of the particle movement, the equations (2) and (3) can be given as

$$\rho \frac{\partial v_i}{\partial t} = \frac{\partial \tau_{ij}}{\partial x_j}, \quad (4)$$

$$\frac{\partial \tau_{ij}}{\partial t} = c_{ijpq} \frac{\partial v_p}{\partial x_q}. \quad (5)$$

We can apply the Fourier transform for the variables ω , x_1 , x_2 to equations (4) and (5) according to the following relations

$$\tilde{f}(p_1, p_2, \omega) = \frac{1}{8\pi^3} \int \int \int_{-\infty}^{\infty} f(x_1, x_2, t) e^{-i\omega(p_1 x_1 + p_2 x_2 - t)} dx_1 dx_2 dt,$$

$$f(x_1, x_2, t) = \int \int \int_{-\infty}^{\infty} \omega^2 \tilde{f}(p_1, p_2, \omega) e^{i\omega(p_1 x_1 + p_2 x_2 - t)} dp_1 dp_2 d\omega.$$

After substituting the derivatives on x_1 , x_2 , t with the coefficients $i\omega p_1$, $i\omega p_2$, $-i\omega$, and excluding the variables τ_{11} , τ_{12} , τ_{22} , the system of equations (4)-(5) can be given in a vector-matrix form

$$\frac{d\mathbf{b}}{dz} = i\omega \mathbf{M} \mathbf{b}, \quad (6)$$

where vector $\mathbf{b} = (v_1, v_2, v_3, \tau_{13}, \tau_{23}, \tau_{33})^T$, $z \equiv x_3$, and matrix \mathbf{M} is defined as

$$\mathbf{M} = - \begin{pmatrix} \mathbf{A} & \mathbf{C}_{33}^{-1} \\ \mathbf{B} & \mathbf{A}^T \end{pmatrix}, \quad (7)$$

with $C_{mn}[p, q] = c_{mp, nq}$, $\mathbf{A} = \mathbf{C}_{33}^{-1}(p_1 \mathbf{C}_{31} + p_2 \mathbf{C}_{32})$ and $\mathbf{B} = \sum_{m, n=1, 2} p_m p_n (\mathbf{C}_{m3} \mathbf{C}_{33}^{-1} \mathbf{C}_{3n} - \mathbf{C}_{mn}) + \rho \mathbf{I}$, where p_1 and p_2 are the horizontal slowness in x_1 and x_2 direction, respectively, and ρ is the density. The matrices \mathbf{C}_{33}^{-1} and \mathbf{B} are symmetrical, and matrix \mathbf{M} satisfies the equation

$$\mathbf{KMK} = \mathbf{M}^T, \quad (8)$$

where \mathbf{M}^T is transposed matrix, $\mathbf{K} = \begin{pmatrix} \mathbf{0} & \mathbf{I} \\ \mathbf{I} & \mathbf{0} \end{pmatrix}$ and \mathbf{I} is the unit 3x3 matrix. Equation (6) describes the wave propagation in the vertically heterogeneous medium with all parameters being dependent on z -coordinate only. Note, even if the parameters $\rho(z)$ and $c_{ijpq}(z)$ are discontinuous functions, the components of the vector \mathbf{b} remain continuous functions of depth. If the medium is a homogeneous transversely isotropic with vertical symmetry axis (a VTI medium), the propagation of waves in qP-qSV system is independent from the qSH-waves propagation. In this case, there are two equations (6): with dimension 4x4 (qP-qSV system) and with dimension 2x2 (qSH wave). For vertical propagation, equation (6) is reduced into three independent equations (for qP-, qSV- and qSH-waves). The analytical form of matrix \mathbf{M} for different types of media can be found in Aki and Richards (1980), Braga and Herrmann (1992) and Fryer and Frazer (1987).

3. Propagator matrix

The propagator matrix is the matrix $\mathbf{P}(z, z_0) \in \mathbf{GL}_6(\mathbf{C})$ that is the solution of initial-value problem

$$\frac{\partial \mathbf{P}(z, z_0)}{\partial z} = i\omega \mathbf{M} \mathbf{P}(z, z_0), \quad \mathbf{P}(z_0, z_0) = \mathbf{I}. \quad (9)$$

The propagator matrix satisfies the Volterra integral equation

$$\mathbf{P}(z, z_0) = \mathbf{I} + \int_{z_0}^z \mathbf{M}(\eta) \mathbf{P}(\eta, z_0) d\eta, \quad (10)$$

that can be solved by using the Picard iteration. This leads to the Peano series for $\mathbf{P}(z, z_0)$ (Peano, 1888; Pease, 1965)

$$\mathbf{P}(z, z_0) = \mathbf{I} + \int_{z_0}^z \mathbf{M}(\eta_1) d\eta_1 + \int_{z_0}^z \mathbf{M}(\eta_1) \int_{z_0}^{\eta_1} \mathbf{M}(\eta_2) d\eta_2 d\eta_1 + \dots \quad (11)$$

The series (11) converges if $\|\mathbf{M}(\eta)\| \leq c$ for all $\eta \in [z_0, z]$, where $\|\dots\|$ is some matrix norm. If $\mathbf{M}(\eta) = \mathbf{M}$, the matrix with constant elements, then equation (11) is reduced to the exponent

$$\mathbf{P}(z, z_0) = \exp[i\omega(z - z_0)\mathbf{M}]. \quad (12)$$

From equation (9), it follows that for any vector $\mathbf{b}(z_0)$, the vector $\mathbf{b}(z) = \mathbf{P}(z, z_0)\mathbf{b}(z_0)$ is the solution of equation (6). By substituting the basis vectors \mathbf{e}_i , $i = 1, 2, 3$, instead of the vector

$\mathbf{b}(z_0)$, we can prove that the columns of matrix $\mathbf{P}(z, z_0)$ are the linear independent solutions of equation (6), i.e. the propagator matrix describes the fundamental system of solutions of equation (6). Since,

$$\mathbf{b}(z_2) = \mathbf{P}(z_2, z_0)\mathbf{b}(z_0) = \mathbf{P}(z_2, z_1)\mathbf{P}(z_1, z_0)\mathbf{b}(z_0), \quad (13)$$

than,

$$\mathbf{P}(z_2, z_0) = \mathbf{P}(z_2, z_1)\mathbf{P}(z_1, z_0). \quad (14)$$

If the medium consists of N layers with matrices \mathbf{M}_i and layer thickness h_i , the equations (12)-(14) gives the propagator matrix from the stack of the layers

$$\mathbf{P}(z_N, z_0) = \exp(i\omega h_N \mathbf{M}_N) \dots \exp(i\omega h_1 \mathbf{M}_1), \quad (15)$$

where $z_N = z_0 + h_1 + \dots + h_N$.

Equation (15) was used by Haskell (1953) and Thomson (1950) in their works to describe the wave propagation in a layered isotropic medium.

4. Symmetry relations

Let us assume that matrices \mathbf{M}_k can be diagonalized by using a similarity transformation, $\mathbf{M}_k = \mathbf{E}_k \text{diag}(\theta_k^{(m)}) \mathbf{E}_k^{-1}$. In this case, $\exp(i\omega h_k \mathbf{M}_k) = \mathbf{E}_k \text{diag}(\exp(i\omega h_k \theta_k^{(m)})) \mathbf{E}_k^{-1}$. The columns of matrix \mathbf{E}_k are the polarization vectors for all types of wave propagating in layer k with horizontal slownesses p_1 and p_2 , while $\theta_k^{(m)}$ are corresponding vertical slownesses. Therefore, the vector $\mathbf{w}(z) = \mathbf{E}_k^{-1} \mathbf{b}(z)$ consists of up- and down-going wave amplitudes in layer k with $h_1 + \dots + h_{k-1} < z < h_1 + \dots + h_k$. Let us denote by \mathbf{E}_0 and \mathbf{E}_{N+1} the matrices that consist of the eigen-vectors of matrices \mathbf{M}_0 and \mathbf{M}_{N+1} , respectively, which define the properties of the half-spaces surrounding the stack of layers. The matrix

$$\mathbf{Q} = \mathbf{E}_{N+1}^{-1} \mathbf{P} \mathbf{E}_0 \quad (16)$$

is called the amplitude propagator matrix, since the equation $\mathbf{w}_{N+1} = \mathbf{Q} \mathbf{w}_0$ provides the linear relation between the amplitudes over and under the stack of layers for all wave types. The amplitude propagator matrix can be blocked by 3x3 sub-matrices, $\mathbf{Q} = (\mathbf{Q}_{ij})_{ij=1,2}$, and the amplitude vectors \mathbf{w}_0 and \mathbf{w}_{N+1} can be blocked by three-component sub-vectors, corresponding to up- and down-going waves of different type,

$$\mathbf{w}_0 = \begin{pmatrix} \mathbf{u}_0 \\ \mathbf{d}_0 \end{pmatrix}, \quad \mathbf{w}_{N+1} = \begin{pmatrix} \mathbf{u}_{N+1} \\ \mathbf{d}_{N+1} \end{pmatrix}. \quad (17)$$

Therefore, we can write

$$\begin{pmatrix} \mathbf{u}_{N+1} \\ \mathbf{d}_{N+1} \end{pmatrix} = \begin{pmatrix} \mathbf{Q}_{11} & \mathbf{Q}_{21} \\ \mathbf{Q}_{21} & \mathbf{Q}_{22} \end{pmatrix} \begin{pmatrix} \mathbf{u}_0 \\ \mathbf{d}_0 \end{pmatrix}. \quad (18)$$

From equation (18), it follows that the amplitudes of waves going away from the stack of layers: \mathbf{u}_0 and \mathbf{d}_{N+1} can be computed from the amplitudes of waves coming to the stack of layers: \mathbf{u}_{N+1} and \mathbf{d}_0 ,

$$\begin{pmatrix} \mathbf{d}_{N+1} \\ \mathbf{u}_0 \end{pmatrix} = \begin{pmatrix} \mathbf{T}_D & \mathbf{R}_U \\ \mathbf{R}_D & \mathbf{T}_U \end{pmatrix} \begin{pmatrix} \mathbf{d}_0 \\ \mathbf{u}_{N+1} \end{pmatrix}, \quad (19)$$

where

$$\mathbf{T}_D = \mathbf{Q}_{22} - \mathbf{Q}_{21} \mathbf{Q}_{11}^{-1} \mathbf{Q}_{12}, \quad (20)$$

$$\mathbf{R}_U = \mathbf{Q}_{21} \mathbf{Q}_{11}^{-1}, \quad (21)$$

$$\mathbf{R}_D = -\mathbf{Q}_{11}^{-1} \mathbf{Q}_{12}, \quad (22)$$

$$\mathbf{T}_U = \mathbf{Q}_{11}^{-1}. \quad (23)$$

The matrices \mathbf{R}_U , \mathbf{T}_U and, \mathbf{R}_D , \mathbf{T}_D are called the reflection and transmission matrices for up- and down-going wave, respectively (Figure 1). From equations (20)-(23), the amplitude propagator matrix can be rewritten as

$$\mathbf{Q} = \begin{pmatrix} \mathbf{T}_U^{-1} & -\mathbf{T}_U^{-1} \mathbf{R}_D \\ \mathbf{R}_U \mathbf{T}_U^{-1} & \mathbf{T}_D - \mathbf{R}_U \mathbf{T}_U^{-1} \mathbf{R}_D \end{pmatrix}. \quad (24)$$

The matrix

$$\mathbf{S} = \begin{pmatrix} \mathbf{T}_D & \mathbf{R}_U \\ \mathbf{R}_D & \mathbf{T}_U \end{pmatrix} \quad (25)$$

is called the scattering matrix (Ursin, 1983) and contains all reflection and transmission coefficients for up- and down-going waves of all type as sub-matrices. If the layers possess the VII (transverse isotropy with vertical symmetry axis) symmetry, the following relation is valid

$$\mathbf{Q}^T \mathbf{J} \mathbf{Q} = \mathbf{J}, \quad (26)$$

where $\mathbf{J} = \begin{pmatrix} \mathbf{0} & \mathbf{I} \\ -\mathbf{I} & \mathbf{0} \end{pmatrix}$. In order to prove the relation (26), we represent the amplitude

propagator matrix \mathbf{Q} as $\mathbf{Q} = \mathbf{F}_N \mathbf{\Lambda}_N \dots \mathbf{\Lambda}_1 \mathbf{F}_0$, where $\mathbf{F}_k = \mathbf{E}_{k+1}^{-1} \mathbf{E}_k$, $\mathbf{\Lambda}_k = \text{diag}(\lambda_k^{(m)})$ and $\lambda_k^{(m)} = \exp(i\omega h_k \theta_k^{(m)})$. To validate the relation (26), it is sufficient to prove that $\mathbf{\Lambda}_k^T \mathbf{J} \mathbf{\Lambda}_k = \mathbf{J}$ and $\mathbf{F}_k^T \mathbf{J} \mathbf{F}_k = \mathbf{J}$. The first equality follows from the fact that the matrix $\mathbf{\Lambda}_k$ is diagonal, and the elements of matrix $\mathbf{\Lambda}_k$ are symmetric, $\lambda_k^{(m+3)} = 1/\lambda_k^{(m)}$. The second equality can be proven by substitution of equations (35) and (36) for matrices \mathbf{E}_k and \mathbf{E}_{k+1}^{-1} into this equation and

using relations (37). The symmetry relations for reflection and transmission matrices for stack of layers sandwiched between two half-spaces,

$$\mathbf{R}_d = \mathbf{R}_d^T, \quad \mathbf{R}_u = \mathbf{R}_u^T, \quad \mathbf{T}_d = \mathbf{T}_u^T, \quad (27)$$

can be derived by substitution the expression for amplitude propagator matrix \mathbf{Q} from equation (24) into equation (26). It is assumed that all layers and half-spaces possess the VTI symmetry, and the presence of attenuation is allowed. The symmetry relations (27) are also derived by Ursin (1983) for a stack of isotropic layers. If we consider the single interface between the half-spaces, then the diagonal sub-matrices in equation (24) are equal (see equations (35) and (36)), and, therefore, $\mathbf{R}_u \mathbf{T}_u^{-1} = -\mathbf{T}_u^{-1} \mathbf{R}_d$ and $\mathbf{T}_u^{-1} = \mathbf{T}_d - \mathbf{R}_u \mathbf{T}_u^{-1} \mathbf{R}_d$ (Ursin, 1983). These relations result in

$$\mathbf{T}_u \mathbf{R}_u + \mathbf{R}_d \mathbf{T}_u = 0, \quad \mathbf{T}_d \mathbf{T}_u + \mathbf{R}_u^2 = \mathbf{I}. \quad (28)$$

By using $\mathbf{R}_u = -\mathbf{T}_u^{-1} \mathbf{R}_d \mathbf{T}_u$ and equations (27) we can derive two additional symmetry relations

$$\mathbf{R}_u \mathbf{T}_d + \mathbf{T}_d \mathbf{R}_d = 0, \quad \mathbf{T}_u \mathbf{T}_d + \mathbf{R}_d^2 = \mathbf{I}. \quad (29)$$

The symmetry relations (28) and (29) are derived by Frasier (1970), Kennett et al. (1978) and Ursin (1983).

5. Reflection and transmission responses of layered transversely isotropic media

This chapter is mostly based on the paper Stovas and Ursin (2003). The major point in this chapter is wave field decomposition into up- and down-going waves (Kennett, 1983; Ursin, 1983) scaled such that, for an elastic medium, the vertical energy flux is constant. This results in important symmetries in the transformation matrix and also in the reflection and transmission (R/T) coefficients (Chapman, 1994; Ursin and Haugen, 1996). The equations of motion and Hook's law in a source free VTI medium (radially symmetric about the vertical, z axis) for qP- and qSV-waves in $X_1 X_3$ plane after applying a Fourier transform can be expressed as an ordinary first-order matrix-vector differential equation as shown in equation (6), where ω denotes circular frequency, $\mathbf{b} = (v_3, \tau_{13}, \tau_{33}, v_1)^T$ is the displacement velocity - stress vector, the superscript "T" indicating the transpose, and the matrix \mathbf{M} has the blocked structure,

$$\mathbf{M} = -\begin{pmatrix} 0 & \mathbf{A} \\ \mathbf{B} & 0 \end{pmatrix}, \quad (30)$$

composed of the 2x2 symmetric matrices \mathbf{A} and \mathbf{B} are given by

$$\mathbf{A} = \begin{pmatrix} c_{33}^{-1} & pc_{13}c_{33}^{-1} \\ pc_{13}c_{33}^{-1} & \rho - p^2(c_{11} - c_{13}^2c_{33}^{-1}) \end{pmatrix}, \quad \mathbf{B} = \begin{pmatrix} \rho & p \\ p & c_{55}^{-1} \end{pmatrix}, \quad (31)$$

which are dependent on the horizontal slowness p , the stiffness coefficients c_{ij} from the stiffness matrix and the density ρ . In order to decompose into up- and down-going waves (Ursin, 1983, Ursin and Stovas, 2002), we make the linear transformation

$$\mathbf{b} = \mathbf{E} \begin{pmatrix} \mathbf{u} \\ \mathbf{d} \end{pmatrix}. \quad (32)$$

Then equation (6) becomes

$$\frac{d}{dz} \begin{pmatrix} \mathbf{u} \\ \mathbf{d} \end{pmatrix} = \left[\begin{pmatrix} -i\omega\Delta & \mathbf{0} \\ \mathbf{0} & i\omega\Delta \end{pmatrix} + \begin{pmatrix} \mathbf{F} & \mathbf{G} \\ \mathbf{G} & \mathbf{F} \end{pmatrix} \right] \begin{pmatrix} \mathbf{u} \\ \mathbf{d} \end{pmatrix}, \quad (33)$$

where \mathbf{u} and \mathbf{d} are the up- and down-going wave amplitudes, and

$$\Delta = \text{diag}(\theta_{qP}, \theta_{qSV}) \quad (34)$$

contains the vertical slownesses for qP- and qSV-waves, θ_{qP} and θ_{qSV} . The transformation matrix

$$\mathbf{E} = \frac{1}{\sqrt{2}} \begin{pmatrix} \mathbf{E}_1 & \mathbf{E}_1 \\ \mathbf{E}_2 & -\mathbf{E}_2 \end{pmatrix} \quad (35)$$

is normalized with respect to the vertical energy flux so that the inverse has the simple form

$$\mathbf{E}^{-1} = \frac{1}{\sqrt{2}} \begin{pmatrix} \mathbf{E}_1^{-1} & \mathbf{E}_2^{-1} \\ \mathbf{E}_1^{-1} & -\mathbf{E}_2^{-1} \end{pmatrix} = \frac{1}{\sqrt{2}} \begin{pmatrix} \mathbf{E}_2^T & \mathbf{E}_1^T \\ \mathbf{E}_2^T & -\mathbf{E}_1^T \end{pmatrix}. \quad (36)$$

Matrices \mathbf{E}_1 and \mathbf{E}_2 possess the symmetries

$$\mathbf{E}_2^T \mathbf{E}_1 = \mathbf{E}_2 \mathbf{E}_1^T = \mathbf{I}. \quad (37)$$

Therefore, the layer propagator matrix can be given as

$$\mathbf{P}_k = \exp(i\omega h \mathbf{M}_k) = \mathbf{E} \exp(i\omega h \Delta) \mathbf{E}^{-1} = \begin{pmatrix} \mathbf{P}_{11}^{(k)} & i\mathbf{P}_{12}^{(k)} \\ i\mathbf{P}_{21}^{(k)} & \mathbf{P}_{11}^{(k)} \end{pmatrix}, \quad (38)$$

where $\mathbf{P}_{mm}^{(k)} = \mathbf{E}_m \cos(\omega h \Delta) \mathbf{E}_m^{-1}$ and $\mathbf{P}_{mn}^{(k)} = \mathbf{E}_m \sin(\omega h \Delta) \mathbf{E}_n^{-1}$, $m \neq n$, $m, n = 1, 2$. From equation (37) and (38), it follows that

$$\mathbf{P}_k^{-1} = \exp(-i\omega h \mathbf{M}_k) = \mathbf{E} \exp(-i\omega h \Delta) \mathbf{E}^{-1} = \begin{pmatrix} \mathbf{P}_{11}^{(k)} & -i\mathbf{P}_{12}^{(k)} \\ -i\mathbf{P}_{21}^{(k)} & \mathbf{P}_{11}^{(k)} \end{pmatrix}, \quad (39)$$

and

$$\begin{aligned} \mathbf{P}_{11}^{(k)T} &= (\mathbf{E}_1 \cos(\omega h \Delta) \mathbf{E}_1^{-1})^T = \mathbf{E}_2 \cos(\omega h \Delta) \mathbf{E}_2^{-1} = \mathbf{P}_{22}^{(k)} \\ \mathbf{P}_{21}^{(k)T} &= (\mathbf{E}_2 \sin(\omega h \Delta) \mathbf{E}_1^{-1})^T = \mathbf{E}_2 \sin(\omega h \Delta) \mathbf{E}_1^{-1} = \mathbf{P}_{21}^{(k)}. \\ \mathbf{P}_{12}^{(k)T} &= (\mathbf{E}_1 \sin(\omega h \Delta) \mathbf{E}_2^{-1})^T = \mathbf{E}_1 \sin(\omega h \Delta) \mathbf{E}_2^{-1} = \mathbf{P}_{12}^{(k)} \end{aligned} \quad (40)$$

The product of matrices of this type indicates that the propagator matrix \mathbf{P} for the stack of layers can be blocked as follows

$$\mathbf{P} = \begin{pmatrix} \mathbf{P}_{11} & i\mathbf{P}_{12} \\ i\mathbf{P}_{21} & \mathbf{P}_{22} \end{pmatrix}, \quad (41)$$

where the elements of 2x2 matrices \mathbf{P}_{kl} are real functions of horizontal slowness p and frequency ω . The elements of matrices $\mathbf{P}_{kl}(\omega)$ are even/odd functions of frequency if $k+l$ is an even/odd number, respectively. Matrix \mathbf{M}_k possesses the following symmetries

$$\mathbf{K}\mathbf{M}_k\mathbf{K} = \mathbf{M}_k^T, \quad \mathbf{T}\mathbf{M}_k\mathbf{T} = -\mathbf{M}_k, \quad (42)$$

where $\mathbf{T} = \begin{pmatrix} \mathbf{I} & \mathbf{0} \\ \mathbf{0} & -\mathbf{I} \end{pmatrix}$. Therefore,

$$\mathbf{K}\mathbf{P}_k\mathbf{K} = \exp(i\omega h\mathbf{M}_k^T) = \mathbf{P}_k^T, \quad \mathbf{T}\mathbf{P}_k\mathbf{T} = \exp(-i\omega h\mathbf{M}_k) = \mathbf{P}_k^{-1}. \quad (43)$$

For an elastic medium, the elements of matrix \mathbf{M}_k are real, and, therefore, $\mathbf{P}_k^* = \mathbf{P}_k^{-1}$, and equations (43) can be rewritten as

$$\mathbf{K}\mathbf{P}_k\mathbf{K} = (\mathbf{P}_k^*)^{-T}, \quad \mathbf{T}\mathbf{P}_k\mathbf{T} = \mathbf{P}_k^*. \quad (44)$$

Multiplications of equations (44) for $k=1, \dots, N$, gives similar symmetry relations for propagator matrix for the stack of layers,

$$\mathbf{K}\mathbf{P}\mathbf{K} = (\mathbf{P}^*)^{-T}, \quad \mathbf{T}\mathbf{P}\mathbf{T} = \mathbf{P}^*. \quad (45)$$

The scattering matrices \mathbf{F} and \mathbf{G} are given by

$$\mathbf{F} = -\frac{1}{2} \left[\mathbf{E}_2^T \frac{d\mathbf{E}_1}{dz} + \mathbf{E}_1^T \frac{d\mathbf{E}_2}{dz} \right], \quad \mathbf{G} = -\frac{1}{2} \left[\mathbf{E}_2^T \frac{d\mathbf{L}_1}{dz} - \mathbf{E}_1^T \frac{d\mathbf{E}_2}{dz} \right], \quad (46)$$

with symmetries

$$\mathbf{F} = -\mathbf{F}^T, \quad \mathbf{G} = \mathbf{G}^T, \quad (47)$$

so that \mathbf{F} and \mathbf{G} have the form

$$\mathbf{F} = \begin{pmatrix} 0 & f \\ -f & 0 \end{pmatrix}, \quad \mathbf{G} = \begin{pmatrix} g_{11} & g_{12} \\ g_{12} & g_{22} \end{pmatrix}. \quad (48)$$

To compute the scattering matrices \mathbf{F} and \mathbf{G} , we express them as functions of perturbations in the elements of the matrices \mathbf{A} and \mathbf{B} in equation (31). The eigenvector matrices satisfy the following equations

$$\mathbf{A}\mathbf{E}_2 = \mathbf{E}_1\Delta, \quad \mathbf{B}\mathbf{E}_1 = -\mathbf{E}_2\Delta. \quad (49)$$

From equations (35) and (36), we obtain

$$\mathbf{E}'_1 = -\mathbf{E}_1(\mathbf{G} + \mathbf{F}), \quad \mathbf{E}'_2 = \mathbf{E}_2(\mathbf{G} - \mathbf{F}). \quad (50)$$

Differentiating equations (49) and substituting equations (50), we obtain

$$\begin{aligned} \Delta \mathbf{G} + \mathbf{G} \Delta &= \begin{pmatrix} 2g_{11}\theta_{qP} & g_{12}(\theta_{qP} + \theta_{qSV}) \\ g_{12}(\theta_{qP} + \theta_{qSV}) & 2g_{22}\theta_{qSV} \end{pmatrix} = -\frac{1}{2}(\mathbf{E}_2^T \mathbf{A}' \mathbf{E}_2 + \mathbf{E}_1^T \mathbf{B}' \mathbf{E}_1) \\ \Delta \mathbf{F} - \mathbf{F} \Delta &= \begin{pmatrix} 0 & f(\theta_{qP} - \theta_{qSV}) \\ f(\theta_{qP} - \theta_{qSV}) & 0 \end{pmatrix} = \frac{1}{2}(\mathbf{E}_2^T \mathbf{A}' \mathbf{E}_2 - \mathbf{E}_1^T \mathbf{B}' \mathbf{E}_1) - \Delta' \end{aligned} \quad (51)$$

From equations (51) we can compute all elements of matrices \mathbf{F} and \mathbf{G} .

Equation (6) can be solved not only by propagator matrix technique described in previous chapter, but also by a layer-recursive scheme described in Ursin and Stovas (2002). We let \mathbf{R}_{Dj} , \mathbf{T}_{Dj} , \mathbf{R}_{Uj} and \mathbf{T}_{Uj} denote the R/T matrices for the interface at $z = z_j$ (Figure 1). For the layer thickness $\Delta z_j = z_j - z_{j-1}$, the layer propagator matrix is given by

$$\mathbf{L}_j = \exp(i\omega \Delta z_j \Lambda_j). \quad (52)$$

Assume that the generalized reflection matrix from the top of layer $j+1$ to the bottom of the stratified medium, $\mathbf{R}_D(z_j^+, z_N^+)$, is known; then the new reflection matrix up to the top of layer j is given by the recursive relation (Ursin, 1983)

$$\mathbf{R}_D(z_{j-1}^+, z_N^+) = \mathbf{L}_j \left\{ \mathbf{R}_{Dj} + \mathbf{T}_{Uj} \mathbf{R}_D(z_j^+, z_N^+) [\mathbf{I} + \mathbf{R}_{Dj} \mathbf{R}_D(z_j^+, z_N^+)]^{-1} \mathbf{T}_{Dj} \right\} \mathbf{L}_j. \quad (53)$$

It is started with the initial value $\mathbf{R}_D(z_j^+, z_N^+) = 0$, satisfying the radiation condition in the elastic half-space. By considering a plane interface between two homogeneous media, we can define the transmission and reflection coefficient matrices. Continuity of the wavefields gives the 2x2 reflection and transmission matrices (Ursin, 1983):

$$\mathbf{T}_D = \begin{pmatrix} t_{DPP} & t_{DPS} \\ t_{DSP} & t_{DSS} \end{pmatrix} = 2(\mathbf{C} + \mathbf{D})^{-1}, \quad \mathbf{R}_D = \begin{pmatrix} r_{DPP} & r_{DPS} \\ r_{DSP} & r_{DSS} \end{pmatrix} = (\mathbf{C} - \mathbf{D})(\mathbf{C} + \mathbf{D})^{-1}, \quad (54)$$

with

$$\mathbf{C} = [\mathbf{E}_2^{(1)}]^T \mathbf{E}_1^{(2)}, \quad \mathbf{D} = [\mathbf{E}_1^{(1)}]^T \mathbf{E}_2^{(2)}, \quad (55)$$

where superscripts ⁽¹⁾ and ⁽²⁾ denote the upper and lower medium, respectively.

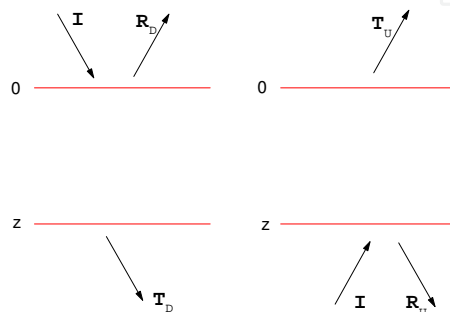


Fig. 1. Definition of the reflection and transmission response matrices (Ursin&Stovas, 2002).

The symmetry equations (37) imply that

$$\mathbf{CD}^T = \mathbf{I}. \quad (56)$$

Using equation (55), the reflection and transmission matrices are given by

$$\mathbf{T}_D = \frac{2}{\det(\mathbf{C} + \mathbf{D})\det\mathbf{C}} \begin{pmatrix} c_{11} + c_{22}\det\mathbf{C} & c_{21} - c_{12}\det\mathbf{C} \\ c_{12} - c_{21}\det\mathbf{C} & c_{22} + c_{11}\det\mathbf{C} \end{pmatrix} \quad (57)$$

$$\mathbf{R}_D = \frac{1}{\det(\mathbf{C} + \mathbf{D})\det\mathbf{C}} \begin{pmatrix} (\det\mathbf{C})^2 - 1 + c_{11}^2 + c_{12}^2 - c_{21}^2 - c_{22}^2 & 2(c_{11}c_{21} + c_{12}c_{22}) \\ 2(c_{11}c_{21} + c_{12}c_{22}) & (\det\mathbf{C})^2 - 1 - c_{11}^2 - c_{12}^2 + c_{21}^2 + c_{22}^2 \end{pmatrix}$$

where c_{ij} are elements of matrix \mathbf{C} and

$$\det(\mathbf{C} + \mathbf{D})\det\mathbf{C} = (\det\mathbf{C})^2 + 1 + c_{11}^2 + c_{12}^2 + c_{21}^2 + c_{22}^2. \quad (58)$$

The matrices \mathbf{R}_U and \mathbf{T}_U can be computed by interchanging the superscripts 1 and 2 or using the symmetry relations (37) and (56) (Ursin and Stovas, 2001), which gives

$$\mathbf{T}_U = \mathbf{T}_D^T, \quad \mathbf{R}_U = -\mathbf{T}_D\mathbf{R}_D\mathbf{T}_D^{-1}. \quad (59)$$

The weak-contrast approximations for reflection and transmission matrices can be derived by assuming weak contrast in elastic parameters above and below the interface. We consider a plane interface with a discontinuity in the parameters

$$\Delta m_k = m_k^{(2)} - m_k^{(1)} \quad (60)$$

and average parameters

$$m_k = \frac{m_k^{(2)} + m_k^{(1)}}{2}, \quad (61)$$

where $m_k^{(1)}$ and $m_k^{(2)}$ characterize the medium above and below the interface, respectively.

To approximate the reflection and transmission matrices in equation (54), we proceed as in Stovas and Ursin (2001) and expand the matrices $\mathbf{E}_k^{(j)}$, $k=1,2$, $j=1,2$, into second-order Taylor series with respect to the average medium. This gives the second-order approximations

$$\mathbf{T}_D^{(2)} \approx \begin{pmatrix} 1 - \frac{1}{2}(g_{11}^2 + g_{12}^2 + f^2) & f - \frac{1}{2}g_{12}(g_{11} + g_{22}) \\ -f - \frac{1}{2}g_{12}(g_{11} + g_{22}) & 1 - \frac{1}{2}(g_{12}^2 + g_{22}^2 + f^2) \end{pmatrix}, \quad \mathbf{R}_D^{(2)} \approx - \begin{pmatrix} g_{11} - g_{12}f & g_{12} + \frac{1}{2}f(g_{11} - g_{22}) \\ g_{12} + \frac{1}{2}f(g_{11} - g_{22}) & g_{22} + g_{12}f \end{pmatrix}. \quad (62)$$

From the symmetries of the matrices \mathbf{E}_1 and \mathbf{E}_2 , the second-order derivatives of these matrices with respect to the medium parameters cancel; therefore they do not appear in the second-order approximations for the R/T coefficients. In the equations above, the elements f and g_{ij} are as defined in equation (46), but the derivatives of the medium parameters $\frac{dm_k}{dz}$ are replaced by Δm_k . Neglecting the second-order terms gives the linear approximations

$$\mathbf{T}_D^{(1)} \approx \mathbf{I} + \mathbf{F}, \quad \mathbf{R}_D^{(1)} \approx -\mathbf{G}. \quad (63)$$

These correspond to ones given in Ursin and Haugen (1996) for VTI media and in Aki and Richards (1980) for isotropic media, except that they are normalized with respect to the vertical energy flux and not with respect to amplitude.

6. Periodically layered media

Let us introduce the infinite periodically layered VTI medium with the period thickness

$H = \sum_{j=1}^N h_j$, where h_j is the thickness of j^{th} layer in the sequence of N layers comprising the period. The dispersion equation for this N layered medium is given by (Helbig, 1984)

$$\det(\mathbf{P} - \exp(i\omega H \theta) \mathbf{I}) = 0, \quad (64)$$

and the period propagator matrix \mathbf{P} is specified by formula (15). The equation (64) is known as the Floquet (1883) equation.

The parameter $\theta = \theta(p, \omega)$ is effective and generally complex vertical component of the slowness vector. For plane waves with horizontal slowness p , the real part of θ which satisfies equation (64), $\text{Re } \theta = q$, defines the vertical slowness of the envelope, while the imaginary part, $\text{Im } \theta = \gamma$, characterizes the attenuation due to scattering. Note that for propagating waves, $\lim_{\omega \rightarrow 0} \gamma = 0$. This indicates that there is no scattering in the low frequency limit.

The low and high frequency limits

In the low-frequency asymptotic of the propagator matrix \mathbf{P} has the following form $\mathbf{P} = \exp(i\omega H \tilde{\mathbf{M}}(\omega))$ with

$$\tilde{\mathbf{M}}(\omega) = \frac{1}{H} \sum_{k=1}^N h_k \mathbf{M}_k + \frac{i\omega}{2H^2} \sum_{j>\ell} h_j h_\ell (\mathbf{M}_j \mathbf{M}_\ell - \mathbf{M}_\ell \mathbf{M}_j) + o(\omega) \quad (65)$$

Therefore, the dispersion equation (64) in the low-frequency limit has roots similar to those defined for a homogeneous VTI medium given by the averaged matrix

$$\tilde{\mathbf{M}}(0) = \frac{1}{H} \sum_{k=1}^N h_k \mathbf{M}_k. \quad (66)$$

One can see from observing the elements of the matrices in equation (31) that equation (66) is equivalent to the Backus averaging. The propagator matrix $\tilde{\mathbf{P}}$, which defines the propagation of mode m_k in the k^{th} layer, $k = 1, \dots, N$, can be defined as

$$\tilde{\mathbf{P}} = \exp(i\omega h_N \mathbf{F}_N) \dots \exp(i\omega h_k \mathbf{F}_k) \dots \exp(i\omega h_1 \mathbf{F}_1), \quad (67)$$

where $\mathbf{F}_k = \theta_k^{(m_k)} \mathbf{n}_k^{(m_k)} \mathbf{m}_k^{(m_k)T}$ is a 4x4 matrix of rank one, $\mathbf{m}_k^{(m_k)T}$ and $\mathbf{n}_k^{(m_k)}$ are the left- and right hand side eigenvectors of matrix \mathbf{M}_k with eigenvalue $\theta_k^{(m_k)}$. Substituting \mathbf{F}_k into equation (67) results in

$$\tilde{\mathbf{P}} = \exp \left[i\omega \sum_{k=1}^N h_k \theta_k^{(m_i)} \right] \left(\mathbf{n}_N^{(m_s)} \mathbf{m}_N^{(m_s)^T} \dots \mathbf{n}_1^{(m_i)} \mathbf{m}_1^{(m_i)^T} \right) = \exp \left[i\omega \sum_{k=1}^N h_k \theta_k^{(m_i)} + \beta \right] \left(\mathbf{n}_N^{(m_s)} \mathbf{m}_1^{(m_i)^T} \right), \quad (68)$$

where the number $\beta = \ln \left(\mathbf{m}_N^{(m_s)^T} \dots \mathbf{n}_1^{(m_i)} \right)$. In this case, the dispersion equation (64), which defines the vertical slowness for the period of the layered medium, has the root given by

$$\theta = \frac{1}{H} \sum_{k=1}^N h_k \theta_k^{(m_i)} - \frac{i\beta}{\omega H}, \quad (69)$$

where the term $i\beta/\omega H$ is responsible for the transmission losses for propagating waves which is frequency independent. This can be shown by considering the single mode plane wave,

$$\exp[i\omega(pr + \theta z - t)] = \exp[i\omega(pr + qz - t)] \exp[\beta z/H], \quad (70)$$

where

$$q = \frac{1}{H} \sum_{k=1}^N h_k q_k^{(m_i)}. \quad (71)$$

This equation defines the vertical slowness for a single mode transmitted wave initiated by a wide-band δ -pulse, since it is frequency-independent. The caustics from multi-layered VTI medium in high-frequency limits are discussed in Roganov and Stovas (2010). Note, that propagator matrix in equation (68) describes the downward plane wave propagation of a given mode within each layer, i.e. the part of the full wave field. All multiple reflections and transmissions of other modes are ignored. Therefore, this notation is valid for the case of the frequency independent single mode propagation of a wide band δ pulse. In the low frequency limit, the wave field consists of the envelope with all wave modes. For an accurate description of this envelope and obtaining the Backus limit we have to use the formula (15) for complete propagator \mathbf{P} .

6.1 Dispersion equation analysis

From the relations (45), one can see that the matrices \mathbf{P} , \mathbf{P}^* and $(\mathbf{P}^*)^{-T}$ are similar. These matrices have the same eigen-values. So, if x is eigen-value of matrix \mathbf{P} , then x^* , x^{-1} and $(x^{-1})^*$ are also eigen-values. Additionally, taking into account the identity, $\det(\mathbf{P})=1$, it can be shown, that equation

$$\det(\mathbf{P} - x\mathbf{I}) = 0 \quad (72)$$

reduces to

$$(x + x^{-1})^2 - a_1(x + x^{-1}) + a_2 - 2 = 0, \quad (73)$$

and the roots of equation (64) corresponding to qP- and qSV-waves, $\pm\theta_p$ and $\pm\theta_s$, satisfy the equations

$$\cos(\omega H \theta_{qP}) + \cos(\omega H \theta_{qSV}) = \frac{1}{2} a_1(p, \omega), \quad \cos(\omega H \theta_{qP}) \cos(\omega H \theta_{qSV}) = \frac{1}{4} a_2(p, \omega) - \frac{1}{2}. \quad (74)$$

The real functions $a_1(p, \omega)$ and $a_2(p, \omega)$ can be computed using the trace and the sum of the principal second order minors of the matrix \mathbf{P} , respectively. Using equation (41) and taking into account that $\mathbf{P}_{11}(\omega)$ and $\mathbf{P}_{22}(\omega)$ are even functions of frequency, and $\mathbf{P}_{12}(\omega)$ and $\mathbf{P}_{21}(\omega)$ are odd functions of frequency, the functions $a_1(p, \omega)$ and $a_2(p, \omega)$ are even functions of frequency and horizontal slowness. The system of equations (74) defines the continuous branches of functions $\pm \text{Re} \theta_{qP} = \pm q_{qP}(p, \omega)$ and $\pm \text{Re} \theta_{qSV} = \pm q_{qSV}(p, \omega)$ which specify the vertical slowness of four envelopes with horizontal slowness p and frequency ω . Let us denote $b_1(p, \omega) = a_1(p, \omega)/4$, $b_2(p, \omega) = a_2(p, \omega)/4 - 1/2$ and $y = \frac{x + x^{-1}}{2}$. Note that the functions $b_1(p, \omega)$ and $b_2(p, \omega)$ are also even functions of frequency and horizontal slowness.

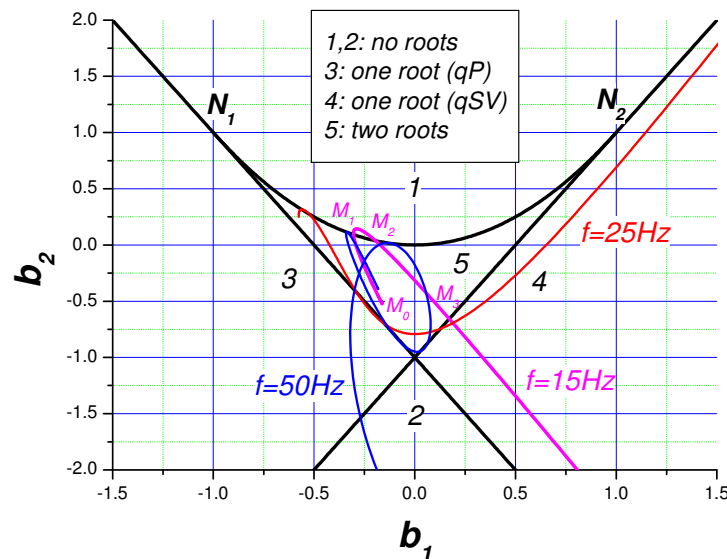


Fig. 2. Propagating and evanescent regions for qP – and qSV – waves in the (b_1, b_2) domain. The points $N_1(-1, 1)$ and $N_2(1, 1)$ denote the crossings between $b_2 = -1 \pm 2b_1$ and $b_2 = b_1^2$. The paths corresponding to $f = \text{const}$ are given for frequencies of $f = 15, 25$ and 50Hz are shown in magenta, red and blue, respectively. The starting point M_0 (that corresponds to zero horizontal slowness) and the points corresponding to crossings of the path and boundaries between the propagating regions, $M_j, j = 1, 2, 3$, are shown for the frequency $f = 15\text{Hz}$. Points M_4 and M_5 are outside of the plotting area (Roganov&Stovas, 2011).

All envelopes are propagating, if the roots of quadratic equation

$$y^2 - 2b_1y + b_2 = 0 \quad (75)$$

are such that $|y_1| \leq 1$ and $|y_2| \leq 1$. On the boundaries between propagating and evanescent envelopes, we have $y = \pm 1$ or discriminator of equation (75), $D(p, \omega) = b_1^2 - b_2 = 0$. In the first case we have, $b_2 = -1 \pm 2b_1$, and in the second case, $b_2 = b_1^2$ (Figure 2). If $|y| > 1$, the equation $y = \cos(\omega H \theta)$ has the following solutions

$$\theta = \pm \frac{1}{\omega H} \left[2\pi n + i \ln \left(y + \sqrt{y^2 - 1} \right) \right], n \in \mathbf{Z}, y > 1$$

$$\theta = \pm \frac{1}{\omega H} \left[(2n+1)\pi + i \ln \left(-y + \sqrt{y^2 - 1} \right) \right], n \in \mathbf{Z}, y < -1$$
(76)

and $q = \text{Re}\theta = \text{const}$ in this area. The straight lines $b_2 = -1 \pm 2b_1$ and the parabola $b_2 = b_1^2$ defined between the tangent points $N_1(-1,1)$ and $N_2(1,1)$ split the coordinate plane (b_1, b_2) into five regions (Figure 2). If parameters b_1 and b_2 are such that the corresponding point (b_1, b_2) is located in region 1 or 2, the system of equations (74) has no real roots, and corresponding envelopes do not contain the propagating wave modes. The envelopes with one propagating wave of qP- or qSV- wave mode correspond to the points located in region 3 or region 4, respectively. The points from region 5 result in envelopes with both propagating qP- and qSV-wave modes. If a specific frequency is chosen, for instance, $\omega = 30\pi \text{Hz}$ (or $f = 15 \text{Hz}$), and only the horizontal slowness is varied, the point with coordinates (b_1, b_2) will move along some curve passing through the different regions. Consequently, the number of propagating wave modes will be changed. In Figure 2, we show using the points M_i ($i = 0, \dots, 5$) with the initial position M_0 defined by $p = 0$ and the following positions crossing the boundaries for the regions occurred at $p_1 = 0.172 \text{s/km}$, $p_2 = 0.217 \text{s/km}$ and $p_3 = 0.246 \text{s/km}$. This curve will also cross the line $b_2 = -1 + 2b_1$ at $p_4 = 0.332 \text{s/km}$ and $p_5 = 0.344 \text{s/km}$. Between the last two points, the curve is located in the region 2 with no propagating waves for both modes. The frequency dependent positions of the stop bands for $p = \text{const}$ can be investigated using the curve, $b(\omega) = [b_1(\omega), b_2(\omega)]$. Since the propagator in the zero frequency limit is given by the identity matrix, $\lim_{\omega \rightarrow 0} \mathbf{P}(\omega) = \mathbf{I}$, then $b_1(0) = b_2(0) = 1$, and all curves $b(\omega)$ start at the point $N_2(1,1)$. For propagating waves, the functions $b_1(\omega)$ and $b_2(\omega)$ are given by linear combinations of trigonometric functions and therefore are defined only in a limited area in the (b_1, b_2) domain.

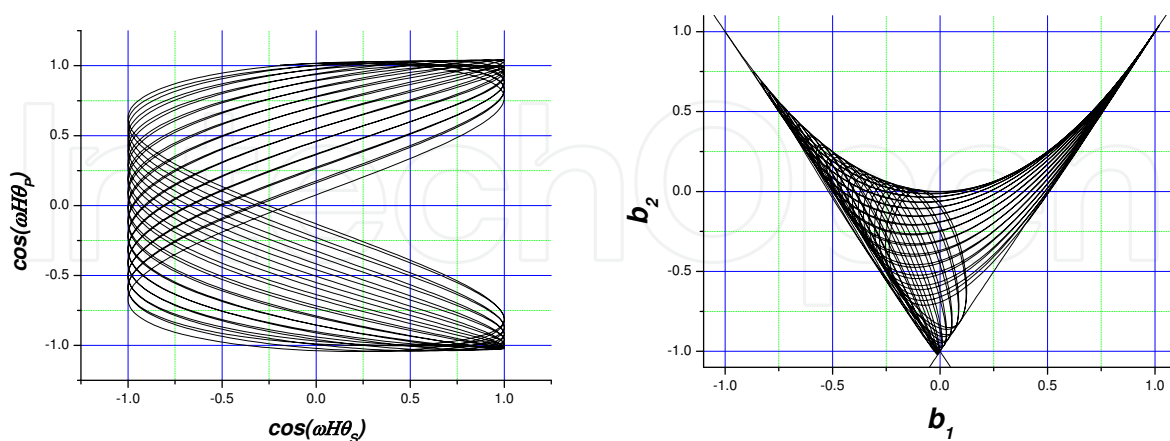


Fig. 3. The normal incidence case ($p = 0$). The dependence of $\cos(\omega H \theta_{qP})$ on $\cos(\omega H \theta_{qSV})$ (a Lissajous curve) is shown (left) and similar curve is plotted in the (b_1, b_2) domain (right). Both of these plots correspond to frequency range $0 - 50 \text{Hz}$. Note, that the stop bands exist only for qP - wave and can be seen for $|\cos(\omega H \theta_{qP})| > 1$ in the left plot and for $b_2 < -1 \pm 2b_1$ in the right one (Roganov&Stovas, 2011).

The simplest case occurs at the normal incidence where $p = 0$. At this point the quadratic equation $y^2 - 2b_1(\omega)y + b_2(\omega) = 0$ has two real roots $y_{qP}(\omega)$ and $y_{qSV}(\omega)$ for each value of ω . The functions $y_{qP}(\omega) = \cos(\omega H \theta_{qP})$ and $y_{qSV}(\omega) = \cos(\omega H \theta_{qSV})$ are the right side of the dispersion equation for qP- and qSV- wave, respectively. If these trigonometric functions have incommensurable periods, the parametric curve $(y_{qSV}(\omega), y_{qP}(\omega))$ densely fills the area that contains rectangle $[-1,1] \times [-1,1]$ and is defined as a Lissajous curve (Figure 3, left). The mapping $(y_{qSV}, y_{qP}) \rightarrow \left(\frac{y_{qSV} + y_{qP}}{2}, y_{qSV} y_{qP} \right)$ has the Jacobian $\left(\frac{y_{qSV} - y_{qP}}{2} \right)$ with a singularity at $y_{qSV} = y_{qP}$. This point is located at the discriminant curve, $b_2 = b_1^2$. We can prove that the curve $\left(\frac{y_{qSV}(\omega) + y_{qP}(\omega)}{2}, y_{qSV}(\omega) y_{qP}(\omega) \right)$ is tangent to parabola $b_2 = b_1^2$ at the singular point and is always located in the region $b_2 \leq b_1^2$. In fact, if $b_1(\omega) = \frac{y_{qSV}(\omega) + y_{qP}(\omega)}{2}$, $b_2(\omega) = y_{qSV}(\omega) y_{qP}(\omega)$ and $y_{qP}(\omega_0) = y_{qSV}(\omega_0)$ then $b_1^2(\omega) - b_2(\omega) = \frac{1}{4} (y_{qP}(\omega) - y_{qSV}(\omega))^2 = 0(\omega - \omega_0)$. In Figure 3 (left), it is shown the parametric curve $(y_{qSV}(\omega), y_{qP}(\omega))$ computed for our two layer model described in Table 1. Since both layers have the same vertical shear wave velocity and density, $y_{qSV}(\omega) = \cos \omega t_{qSV}$ with $t_{qSV} = (h_1 + h_2) / \beta_0$. In the qP- wave case, $y_{qP}(\omega) = \left(\cos \omega (t_{qP1} + t_{qP2}) - r \cos \omega (t_{qP1} - t_{qP2}) \right) / (1 - r^2)$ where $t_{qP1} = h_1 / \alpha_{01}$, $t_{qP2} = h_2 / \alpha_{02}$ and $r = (\alpha_{02} - \alpha_{01}) / (\alpha_{01} + \alpha_{02})$. The solutions of this equation and has been studied by Stovas and Ursin (2007) and Roganov and Roganov (2008). The plot of this curve in (b_1, b_2) domain is shown in Figure 3 (right). It can be seen that the stop bounds are characterized by the values $b_2 < -1 \pm 2b_1$. If $D(p, \omega) < 0$, equation (64) has the complex conjugate and dual roots. Let us denote one of them as $y_1 \in \mathbf{C}$. Then, equation (74) has four complex roots: θ , $-\theta$, θ^* and $-\theta^*$, where $\cos(\omega H \theta) = y_1$. In these cases, the energy envelope equals zero. The up going and down going wave envelopes have different signs for $\gamma = \text{Im} \theta$ that correspond to exponentially damped and exponentially increasing terms.

6.2 Computational aspects

The computation of the slowness surface at different frequencies is performed by computing the propagator matrix (15) for the entire period and analysis of eigenvalues of this matrix. To define the direction for propagation of the envelope with eigenvectors $\mathbf{b} = (v_3, \tau_{13}, \tau_{33}, v_1)^T$ and non-zero energy is done in accordance with sign of the vertical energy flux (Ursin, 1983; Carcione, 2001)

$$E = -\frac{1}{2} \text{Re}(v_1 \tau_{13}^* + v_3 \tau_{33}^*). \quad (77)$$

If $E = 0$, the direction of the envelope propagation depends on the absolute value of $\exp(i\omega H\theta)$; $|\exp(i\omega H\theta)| > 1$ (up going envelope) and $|\exp(i\omega H\theta)| < 1$ (down going envelope). The mode of envelope can be defined by computing the amplitude propagators

$$\mathbf{Q} = \mathbf{E}_1 \mathbf{P} \mathbf{E}_1^{-1}. \quad (78)$$

The absolute values of the elements of the matrix \mathbf{Q} are the amplitudes of the different wave modes composing the envelope and defined in the first layer within the period. Therefore, the envelope of a given mode contains the plane wave of the same mode with the maximum amplitude (when compared with other envelopes).

6.3 Asymptotic analysis of caustics

Let us investigate the asymptotic properties for the vertical slowness of the envelope in the neighborhood of the boundary between propagating and evanescent waves when approaching this boundary from propagating region.

If $y(p_0) = 1$ and $dy/dp_0 = \alpha \neq 0$, than in the neighborhood of the point $p = p_0$ the following approximation of equation $y = \cos(\omega H\theta)$ is valid

$$1 - \frac{\omega^2 H^2 d\theta^2}{2} \approx 1 + \alpha dp, \quad (79)$$

where $dp = p - p_0$, $d\theta = \theta - \theta_0$ and $\theta_0 = \theta(p_0)$. Therefore, $d\theta = O(\sqrt{dp})$, $d\theta/dp = O(1/\sqrt{dp})$, and the curve $\theta(p)$ at the $p = p_0$ has the vertical tangent line, $\lim_{p \rightarrow p_0} (d\theta/dp) = \pm\infty$. In the group space $(x, t(x))$, it leads to an infinite branch represented by caustic. In the area of propagating waves, we have $\lim_{p \rightarrow p_0} (d\theta/dp) = -\infty$. Therefore, $x(p) = -H(d\theta/dp) \rightarrow +\infty$ and $t(p) = H\theta(p) + px(p) \rightarrow +\infty$. Furthermore, for large values of x , $t(x) = p_0 x + H\theta(p_0)$. This fact follows from existence of limit, $\lim_{p \rightarrow p_0} (\theta(p)) = \theta(p_0)$. As a consequence, every continuous branch of the slowness surface limited by the attenuation zones (stop bands) results in the caustic in group space which looks like an open angle sharing the same vertex (Figure 4). When we move from one point of discontinuity to another in the increasing direction of p , the plane angle figure rotates clockwise since the slope of the traveltime curve $dt/dx = p_0$ is increasing. The case where $y(p_0) = -1$ can be discussed in the same manner. If $D(p_0) = 0$, than $\cos(\omega h\theta) = b_1 \pm \sqrt{D(p)} = b_1 \pm O(\sqrt{p})$. Therefore, the asymptotic behavior of $\theta(p)$ as $p \rightarrow p_0$ is the same as discussed above.

6.4 Low frequency caustics

In Figure 5 we show the propagating, evanescent and caustic regions in $p - f$ domain for qP- and qSV- waves ($f = \omega/2\pi$). Figure 5 displays contour plots of the vertical energy flux in the $p - f$ domain for qP- and qSV- waves.

From Figure 5 one can see that the caustic area has weak frequency dependence in the low frequency range (almost vertical structure for caustic region in (p, f) domain, Figures 5 and 6). This follows from more general fact that for VTI periodic medium, $\theta(\omega)$ is even function

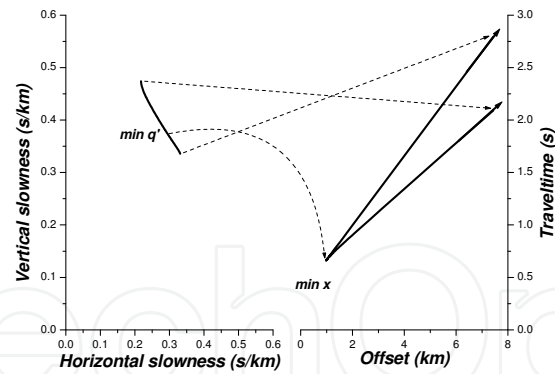


Fig. 4. Sketch for the stop band limited branch of the slowness surface and corresponding branch on the travelttime curve. The correspondence between characteristic points is shown by dotted line (Roganov&Stovas, 2011).

of frequency. Last statement is valid because $y(\omega)$ satisfies the equation (75) and functions $y(\omega) = \cos(\omega H\theta)$, $b_1(\omega)$ and $b_2(\omega)$ are even. Therefore,

$$\theta(\omega) = \theta(0) + o(\omega), \quad (80)$$

and the slowness surface at low frequencies is almost frequency independent.

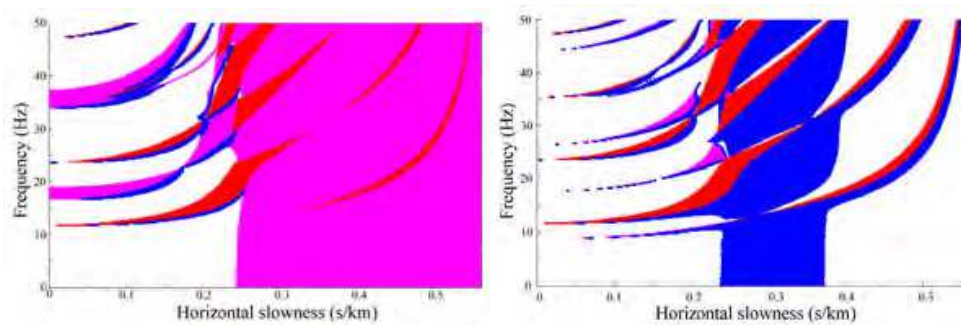


Fig. 5. The propagating, evanescent and caustic regions for the qP – wave (left) and the qSV – wave (right) are shown in the (p, f) domain. The regions are indicated by colors: red – no waves, white – both waves, magenta – qSV – wave only and blue – caustic (Roganov&Stovas, 2011).

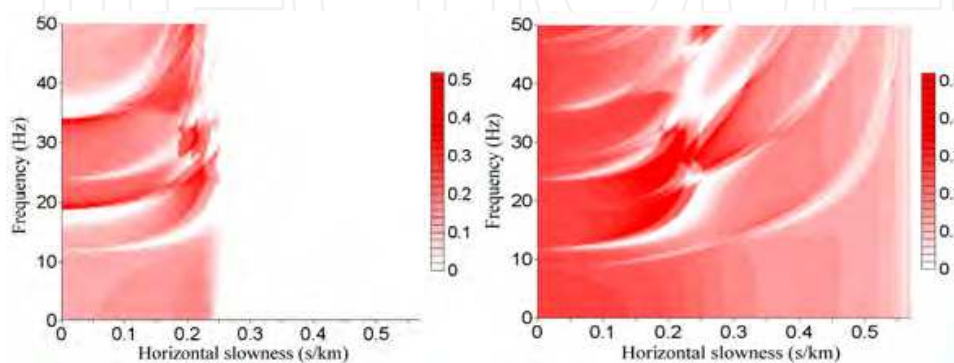


Fig. 6. The vertical energy flux for qP – wave (left) and qSV - wave (right) shown in the (p, f) domain. The zero energy flux zones correspond to evanescent waves (Roganov&Stovas, 2011).

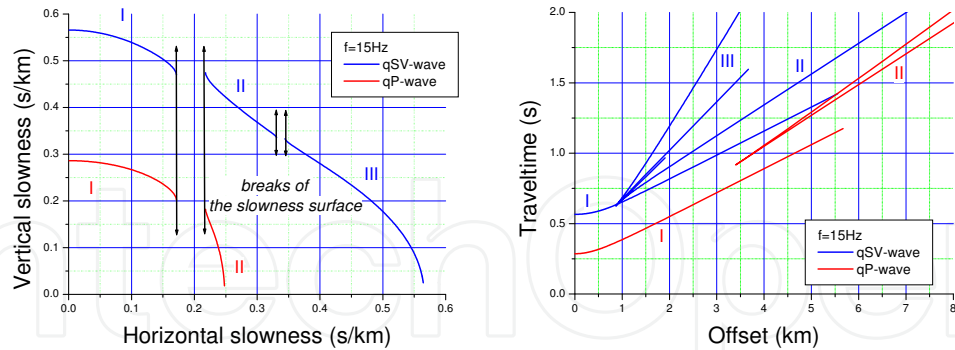


Fig. 7. The qP – and qSV – wave slowness surfaces (left) and the corresponding traveltime curves (right) corresponding frequency of 15Hz . The branches on the slowness surfaces and on the traveltime curves are denoted by I, II and III (for the qSV – wave) and I and II (for the qP – wave) (Roganov&Stovas, 2011).

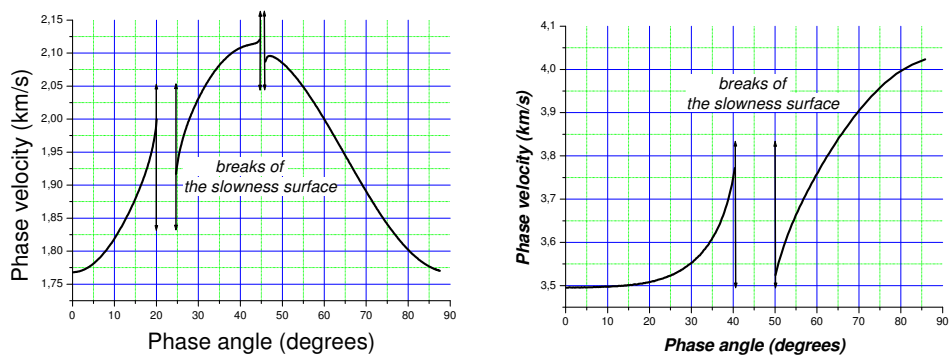


Fig. 8. The phase velocities for qSV – wave (left) and qP – wave (right) computed for a frequency of 15Hz (Roganov&Stovas, 2011).

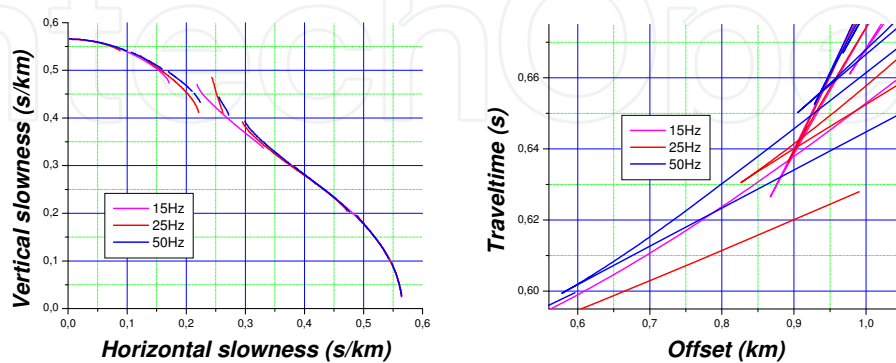


Fig. 9. Comparison of the qSV – slowness surface and traveltime curves computed for frequencies of $f = 15, 25$ and 50Hz (shown in magenta, red and blue colors, respectively) (Roganov&Stovas, 2011).

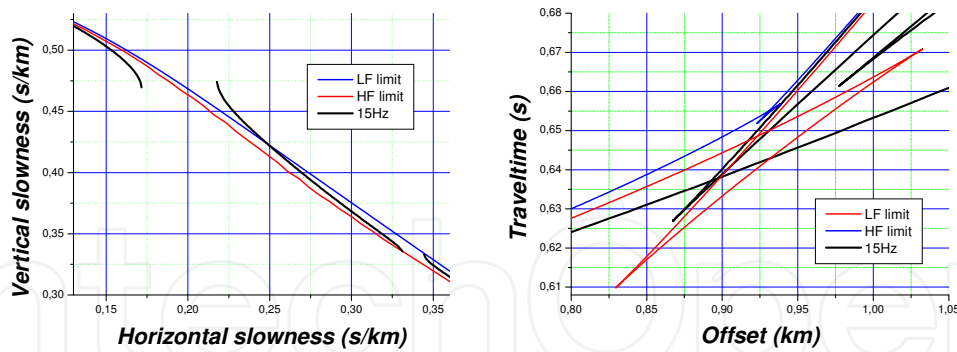


Fig. 10. Comparison of the qSV – slowness surfaces and traveltime curves computed for frequencies of 15, low and high frequency limits (shown in black, red and blue, respectively). Note, the both effective media in low and high frequency limits have triplications for traveltime curves (Roganov&Stovas, 2011).

To illustrate the method described above we choose two-layer transversely isotropic medium with vertical symmetry axis which we used in our previous paper (Roganov and Stovas, 2010). The medium parameters are given in Table 1. Each single VTI layer in the model has its own qSV - wave triplication. In Figure 7 (left), we show the slowness surfaces for the qP - and qSV - waves computed for a single frequency of 15 Hz. The discontinuities in both slowness surfaces correspond to the regions with evanescent waves or zero vertical energy flux, $E = 0$ (equation (77)). The first discontinuity has the same location on the slowness axis for both qP - and qSV - wave slowness surfaces. In the group space (Figure 7, right), we can identify each traveltime branch with correspondent branch of the slowness surface. In Figure 8, we show the phase velocities for qP - and qSV - waves versus the phase angle ψ . The discontinuities in the phase velocity are clearly seen for both qP - and qSV - waves in different phase angle regions. Comparisons of the qSV - wave slowness surface and traveltime curves computed for different frequencies, $f = 15, 25$ and 50Hz are given in Figure 9. One can see that higher frequencies result in more discontinuities in the slowness surface. Only the branches near the vertical and horizontal axis remain almost the same. In Figure 10, we show the slowness surfaces and traveltime curves computed for frequency $f = 15\text{Hz}$ and those computed in the low and high frequency limits. The vertical slowness and traveltime computed in low and high frequency limits are continuous functions of horizontal slowness and offset, respectively.

7. Reflection/transmission responses in periodically layered media

The problem of reflection and transmission responses in a periodically layered medium is closely related to stratigraphic filtering (O'Doherty and Anstey, 1971; Schoenberger and Levin, 1974; Morlet et al., 1982a, b; Banik et al., 1985a, b; Ursin, 1987; Shapiro et al., 1996; Ursin and Stovas, 2002; Stovas and Ursin, 2003; Stovas and Arntsen, 2003). Physical experiments were performed by Marion and Coudin (1992) and analyzed by Marion et al (1994) and Hovem (1995). The key question is the transition between the applicability of low- and high-frequency regimes based on the ratio between wavelength (λ) and thickness (d) of one cycle in the layering. According to different literature sources, this transition

occurs at a critical λ/d value which Marion and Coudin (1992) found to be equal to 10. Carcione et al. (1991) found this critical value to be about 8 for epoxy and glass and to be 6 to 7 for sandstone and limestone. Helbig (1984) found a critical value of λ/d equal to 3. Hovem (1995) used an eigenvalue analysis of the propagator matrix to show that the critical value depends on the contrast in acoustic impedance between the two media. Stovas and Arntsen (2003) showed that there is a transition zone from effective medium to time-average medium which depends on the strength of the reflection coefficient in a finely layered medium.

To compute the reflection and transmission responses, we consider a 1D periodically layered medium. Griffiths and Steinke (2001) have given a general theory for wave propagation in periodic layered media. They expressed the transmission response in terms of Chebychev polynomials of the second degree which is a function of the elements of the propagator matrix for the basic two-layer medium. They also provided an extensive reference list.

7.1 Multi-layer transmission and reflection responses

We consider one cycle of a binary medium with velocities v_1 and v_2 , densities ρ_1 and ρ_2 and the thicknesses h_1 and h_2 as shown in Figure 11. For a given frequency f the phase factors are: $\theta_k = 2\pi fh_k/v_k = 2\pi f \Delta t_k$, where Δt_k is the traveltime in medium k for one cycle. The normal incidence reflection coefficient at the interface between the layers is given by

$$r = \frac{\rho_2 v_2 - \rho_1 v_1}{\rho_2 v_2 + \rho_1 v_1}. \quad (81)$$

The amplitude propagator matrix for one cycle is computed for an input at the bottom of the layers (Hovem, 1995)

$$\mathbf{Q} = \frac{1}{1-r^2} \begin{pmatrix} e^{i\theta_1} & 0 \\ 0 & e^{-i\theta_1} \end{pmatrix} \begin{pmatrix} 1 & r \\ r & 1 \end{pmatrix} \begin{pmatrix} e^{i\theta_2} & 0 \\ 0 & e^{-i\theta_2} \end{pmatrix} \begin{pmatrix} 1 & -r \\ -r & 1 \end{pmatrix} = \begin{pmatrix} a & b \\ b^* & a^* \end{pmatrix}, \quad (82)$$

and

$$a = \frac{e^{i(\theta_1+\theta_2)}(1-r^2 e^{-2i\theta_2})}{1-r^2}, \quad b = -\frac{r e^{i(\theta_1+\theta_2)}(1-e^{-2i\theta_2})}{1-r^2} = \frac{2ir \sin \theta_2}{1-r^2} e^{i\theta_1}. \quad (83)$$

We also compute the real and imaginary part of a (Brekhovskikh, 1960) and absolute value of b , resulting in

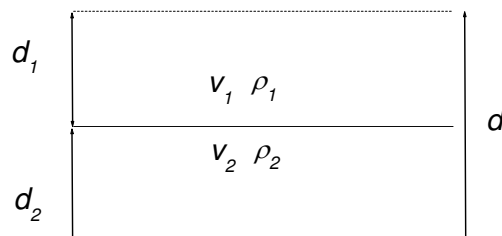


Fig. 11. Single cycle of the periodic medium (Stovas&Ursin, 2007).

$$\begin{aligned}\operatorname{Re} a &= \cos(\theta_1 + \theta_2) - \frac{2r^2}{1-r^2} \sin \theta_1 \sin \theta_2 = \cos \theta_1 \cos \theta_2 - \frac{1+r^2}{1-r^2} \sin \theta_1 \sin \theta_2 \\ \operatorname{Im} a &= \sin(\theta_1 + \theta_2) + \frac{2r^2}{1-r^2} \cos \theta_1 \sin \theta_2 = \sin \theta_1 \cos \theta_2 + \frac{1+r^2}{1-r^2} \cos \theta_1 \sin \theta_2\end{aligned}\quad (84)$$

$$|b| = \frac{2r \sin \theta_2}{1-r^2}$$

We note, that $\det \mathbf{Q} = |a|^2 - |b|^2 = 1$ as shown also by Griffiths and Steinke (2001). The amplitude propagator matrix can be represented by the eigenvalue decomposition (Hovem, 1995)

$$\mathbf{Q} = \mathbf{E} \mathbf{\Sigma} \mathbf{E}^{-1}, \quad (85)$$

where $\mathbf{\Sigma} = \operatorname{diag}[\sigma_1, \sigma_2]$ with

$$\sigma_{1,2} = \begin{cases} \operatorname{Re} a \pm i\sqrt{1 - (\operatorname{Re} a)^2} & \text{for } |\operatorname{Re} a| < 1 \\ \operatorname{Re} a \mp \sqrt{(\operatorname{Re} a)^2 - 1} & \text{for } |\operatorname{Re} a| \geq 1 \end{cases} \quad (86)$$

and the matrix

$$\mathbf{E} = \begin{pmatrix} 1 & 1 \\ (\sigma_1 - a)/b & (\sigma_2 - a)/b \end{pmatrix} \quad (87)$$

A stack of M cycles of total thickness $D = Mh = M(h_1 + h_2)$ has the propagator matrix

$$\mathbf{Q}(M) = \mathbf{Q}^M = \mathbf{E} \mathbf{\Sigma}^M \mathbf{E}^{-1} = \frac{1}{u_{22} - u_{21}} \begin{pmatrix} \sigma_1^M u_{22} - \sigma_2^M u_{21} & \sigma_2^M - \sigma_1^M \\ -u_{21} u_{22} (\sigma_2^M - \sigma_1^M) & \sigma_2^M u_{22} - \sigma_1^M u_{21} \end{pmatrix} \quad (88)$$

with $u_{21} = (\sigma_1 - a)/b$ and $u_{22} = (\sigma_2 - a)/b$. Another way to compute the propagator or transfer matrix is to exploit the Cailey-Hamilton theorem to establish relation between \mathbf{Q}^2 and \mathbf{Q} (Wu et al., 1993) which results in the recursive relation for Chebychev polynomials. The transmission and reflection responses for a down-going wave at the top of the layers are (Ursin, 1983)

$$t_D = p_{22}^{-1} = \frac{\sigma_2 - \sigma_1}{(\sigma_2 - a)\sigma_2^M - (\sigma_1 - a)\sigma_1^M}, \quad r_D = p_{12} p_{22}^{-1} = \frac{(\sigma_2^M - \sigma_1^M)b}{(\sigma_2 - a)\sigma_2^M - (\sigma_1 - a)\sigma_1^M} \quad (89)$$

with p_{ij} , $i, j = 1, 2$ being the elements of propagator matrix $\mathbf{Q}(M)$ given in (88). After algebraic manipulations equation (89) can be written as

$$t_d = \frac{\sin \varphi}{\sin \varphi \cos M \varphi - i \operatorname{Im} a \sin M \varphi} = \frac{\cos M \varphi + i \sin M \varphi \frac{\operatorname{Im} a}{\sin \varphi}}{1 + \sin^2 M \varphi \left[\left(\frac{\operatorname{Im} a}{\sin \varphi} \right)^2 - 1 \right]} = \frac{e^{i\alpha}}{\sqrt{1 + C^2}}, \quad (90)$$

$$r_d = \frac{b \sin M \varphi}{\sin \varphi \cos M \varphi - i \operatorname{Im} a \sin M \varphi} = t_d b \frac{\sin M \varphi}{\sin \varphi} = \frac{C e^{i\left(\alpha + \theta + \frac{\pi}{2}\right)}}{\sqrt{1 + C^2}}$$

where α and C are the phase and amplitude factors, respectively, and φ is the phase of the eigen-value. The equation for transmission response in periodic structure was apparently first obtained in the quantum mechanics (Cvetich and Picman, 1981) and has been rediscovered several times. For extensive discussion see reference 13 in Griffiths and Steinke (2001). The reflection and transmission response satisfy

$$|t_d|^2 + |r_d|^2 = 1, \quad (91)$$

which is conservation of energy. When $|\operatorname{Re} a| < 1$, the eigen-values give a complex phase-shift, representing a propagating regime. Then equation (86) gives

$$\sigma_{1,2} = e^{\pm i\varphi} \quad (92)$$

with $\cos \varphi = \operatorname{Re} a$, which may be obtained from Floquet solution for periodic media, but for first time appeared in Brekhovskikh (1960), equation (7.25). Then we use

$$\cos \alpha = \frac{\cos M \varphi}{\sqrt{1 + C^2}}, \quad C = |b| \frac{\sin M \varphi}{\sin \varphi}, \quad (93)$$

in equation (90). Equation (93) for the amplitude factor is given in a form of Chebychev polynomials of the second kind written in terms of sinusoidal functions. When $|\operatorname{Re} a| > 1$, the eigen-values are a damped or increasing exponential function, representing an attenuating regime. Then equation (86) gives

$$\sigma_{1,2} = e^{\mp \varphi} \quad (94)$$

with $\cosh \varphi = \operatorname{Re} a$. Then the reflection and transmission responses are still given by equation (90) but with phase and amplitude factors now given by

$$\cos \alpha = \frac{\cosh M \varphi}{\sqrt{1 + C^2}}, \quad C = |b| \frac{\sinh M \varphi}{\sinh \varphi}, \quad (95)$$

For the limiting cases with $|\operatorname{Re} a| = 1$, there is a double root

$$\sigma_{1,2} = \operatorname{Re} a \quad (96)$$

and then we must use

$$\cos \alpha = \frac{1}{\sqrt{1 + |b|^2 M^2}}, \quad C = |b| M \quad (97)$$

Note, that in this case $|b|^2 = (\text{Im } a)^2$. To compute expressions (93) and (95) for even number M we use (Gradshteyn and Ryzhik, 1995, equation 1.382)

$$\cos \alpha = \frac{1}{\sqrt{1 + C^2}} \prod_{k=1}^{\frac{M}{2}} \left(1 - \frac{1 - (\text{Re } a)^2}{\sin^2 \frac{(2k-1)\pi}{2M}} \right), \quad C = |b| M (\text{Re } a) \prod_{k=1}^{\frac{M-2}{2}} \left(1 - \frac{1 - (\text{Re } a)^2}{\sin^2 \frac{k\pi}{M}} \right) \quad (98)$$

The transmission response from equation (84) can be expressed via the complex phase factor $\beta(\omega)$:

$$t_D(\omega) = e^{i\beta(\omega)} \quad (99)$$

with

$$\beta(\omega) = \alpha(\omega) + \frac{1}{2} i \ln(1 + C^2). \quad (100)$$

The angular wavenumber is denoted k . With $kD = \text{Re } \beta(\omega)$ or $\cos kD = \cos \alpha(\omega)$, the phase velocity is given by

$$v(\omega) = \omega/k = D\omega/\alpha(\omega). \quad (101)$$

Using notations from Carcione (2001), the dispersion equation can be written as $F(k, \omega) = \cos kD - \cos \alpha(\omega) = 0$, and the expression for group velocity is

$$V(\omega) = -\frac{\partial F/\partial k}{\partial F/\partial \omega} = \frac{D}{\partial \alpha(\omega)/\partial \omega}. \quad (102)$$

7.2 Equivalent time-average and effective medium

The behaviour of the reflection and transmission responses is determined by $\text{Re } a$ which is one for $f = 0$. The boundaries between a propagating and attenuating regime are at $\text{Re } a = -1$ (see equation (84)) given by the equation

$$\tan \frac{\theta_1}{2} \tan \frac{\theta_2}{2} = \frac{1 \mp |r|}{1 \pm |r|}. \quad (103)$$

For low frequencies the stack of the layers behaves as an effective medium with a velocity defined by (Backus, 1962; Hovem, 1995) and can be defined as the zero-frequency limit ($v_{EF} = v(\omega \rightarrow 0)$) from equation (101))

$$\frac{1}{v_{EF}^2} = \frac{1}{v_{TA}^2} + \frac{4h_1h_2}{h^2} \frac{1}{v_1v_2} \frac{r^2}{1-r^2}. \quad (104)$$

This occurs for frequencies below the first root of the equation $\text{Re } a = -1$. For higher frequencies the stack of the layers is characterized by the time-average velocity defined by the infinite frequency limit ($v_{TA} = v(\omega \rightarrow \infty)$ from equation (101))

$$\frac{1}{v_{TA}} = \frac{1}{h_1 + h_2} \left(\frac{h_1}{v_1} + \frac{h_2}{v_2} \right). \quad (105)$$

This occurs for frequencies above the second root of the equation $\text{Re } a = -1$. There is a transition zone between these two roots in which the stack of layers partly blocks the transmitted wave.

The behaviour of the medium is characterized by the ratio between wavelength and layer thickness. This is given by

$$\gamma = \frac{\lambda}{h} = \frac{v_{TA}}{f(h_1 + h_2)} = \frac{1}{f\Delta t}, \quad (106)$$

where Δt is the traveltime through the two single layers. To estimate the critical ratio of wavelength to layer thickness we assume $\Delta t_1 = \Delta t_2 = \Delta t/2$. The effective medium limit the occurs at

$$\gamma_1 = \pi \left(a \tan \sqrt{\frac{1-|r|}{1+|r|}} \right)^{-1}, \quad (107)$$

and the time-average limit the occurs at

$$\gamma_2 = \pi \left(\frac{\pi}{2} - a \tan \sqrt{\frac{1-|r|}{1+|r|}} \right)^{-1}, \quad (108)$$

For small values of $|r| \ll 1$ we obtain

$$\gamma_{1,2} = \pi \left(\frac{\pi}{4} \mp a \tan \frac{|r|}{2} \right)^{-1} \approx 4 \left(1 \pm \frac{2|r|}{\pi} \right). \quad (109)$$

The transition between an effective medium to time average medium is schematically illustrated in Figure 12. Since the boundaries for the transmission zone in equation (103) are periodic functions of frequency, the low wavelength zone (high frequencies) is more complicated than shown in this figure.

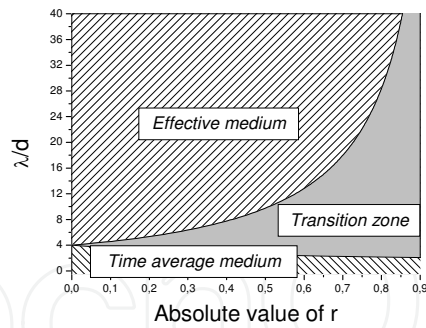


Fig. 12. Schematic representation of the critical $\gamma = \lambda/d$ ratio as function of reflection coefficient ($\theta_1 = \theta_2$) (Stovas&Ursin, 2007).

7.3 Reflection and transmission responses versus layering and layer contrast

We use a similar model as in Marion and Coudin (1992) with three different reflection coefficients: the original $r=0.87$ and $r=0.48$ and $r=0.16$. We use m and Hz instead of mm and kHz . The total thickness of the layered medium is $D = M_k h_k = 51 m$ is constant. M_k , $k = 1, 2, 4, \dots, 64$ is the number of cycles in the layered medium, so that the individual layer thickness is decreasing as k is increasing. The ratio $\theta_1/\theta_2 = \Delta t_1/\Delta t_2 = (h_1 v_2)/(h_2 v_1) = 0.91$. The other model parameters are given in Stovas and Ursin (2007).

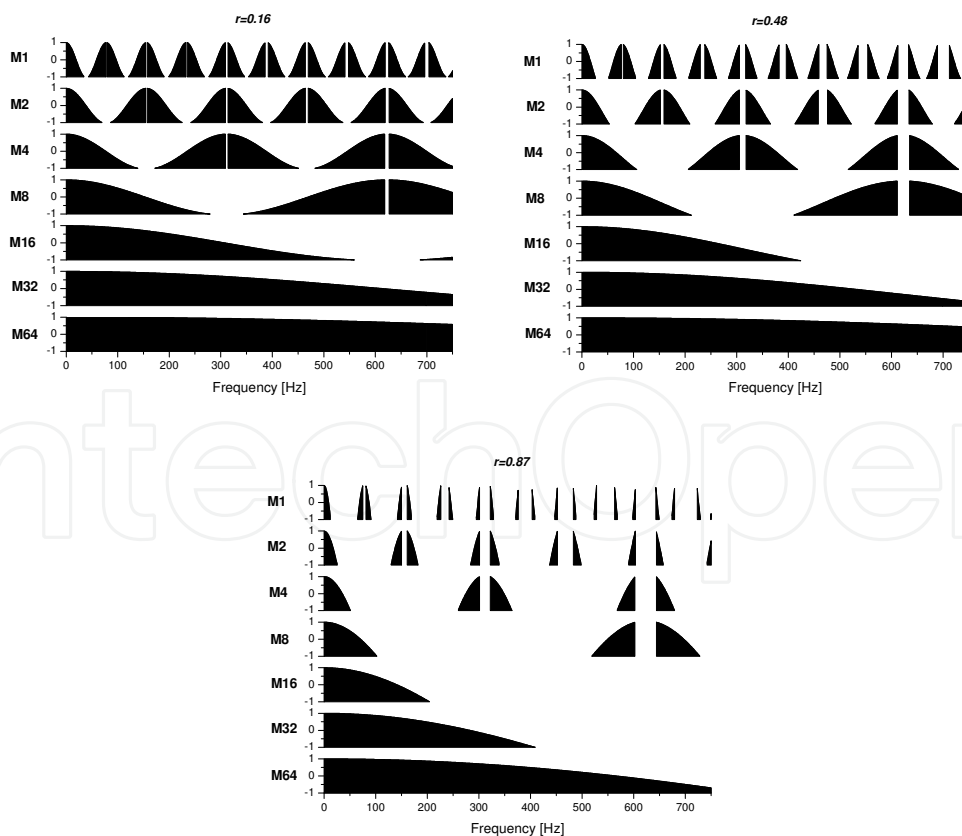


Fig. 13. $\text{Re } a$ as function of frequency. $|\text{Re } a| < 1$ is only plotted with area filled under the curve (Stovas&Ursin, 2007).

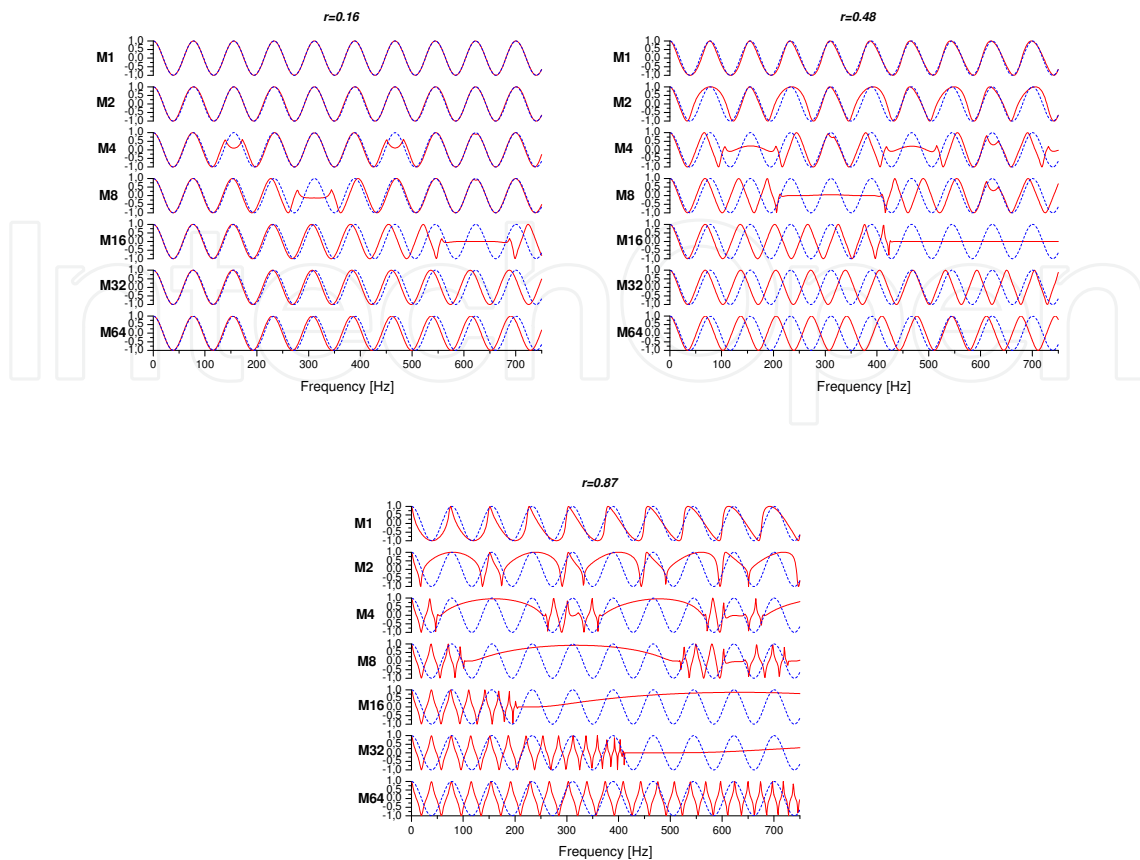


Fig. 14. The phase function $\cos \alpha$ as a function of frequency (from equation (98)) shown by solid line and $\cos \alpha$ corresponding to the single layer with time-average velocity shown by dashed line (Stovas&Ursin, 2007).

The very important parameter that controls the regime is $\text{Re } a$ (equation (84)). The plots of $\text{Re } a$ versus frequency are given in Figure 13 for different models. One can see that the propagating and attenuating regimes are periodically repeated in frequency. The higher reflectivity the more narrow frequency bands are related to propagating regime ($\text{Re } a > -1$). One can also follow that the first effective medium zone is widening as the index of model increases and reflection coefficient decreases, and that the wavelength to layer thickness ratio γ is the parameter which controls the regime. The gaps between the propagating regime bands become larger with increase of reflection coefficient. These gaps correspond to the blocking or attenuating regime. The graphs for the phase factor $\cos \alpha$ and amplitude factor C (equation (98)) are shown in Figure 14 and 15, respectively. The dotted lines in Figure 14 correspond to the time-average phase behaviour. One can see when the computed phase becomes detached from the time-average phase. Note also the anomalous phase behaviour in transition zones. The amplitude factor C (Figure 15) has periodic structure, and periodicity increase with increase of reflection coefficient. In transition zones the amplitude factor reaches extremely large values which correspond to strong dampening. The transmission and reflection amplitudes are shown in Figure 16. The larger reflection coefficient the more frequently amplitudes change with frequency. The transition zones can be seen by attenuated values for transmission amplitudes. With increase of reflection

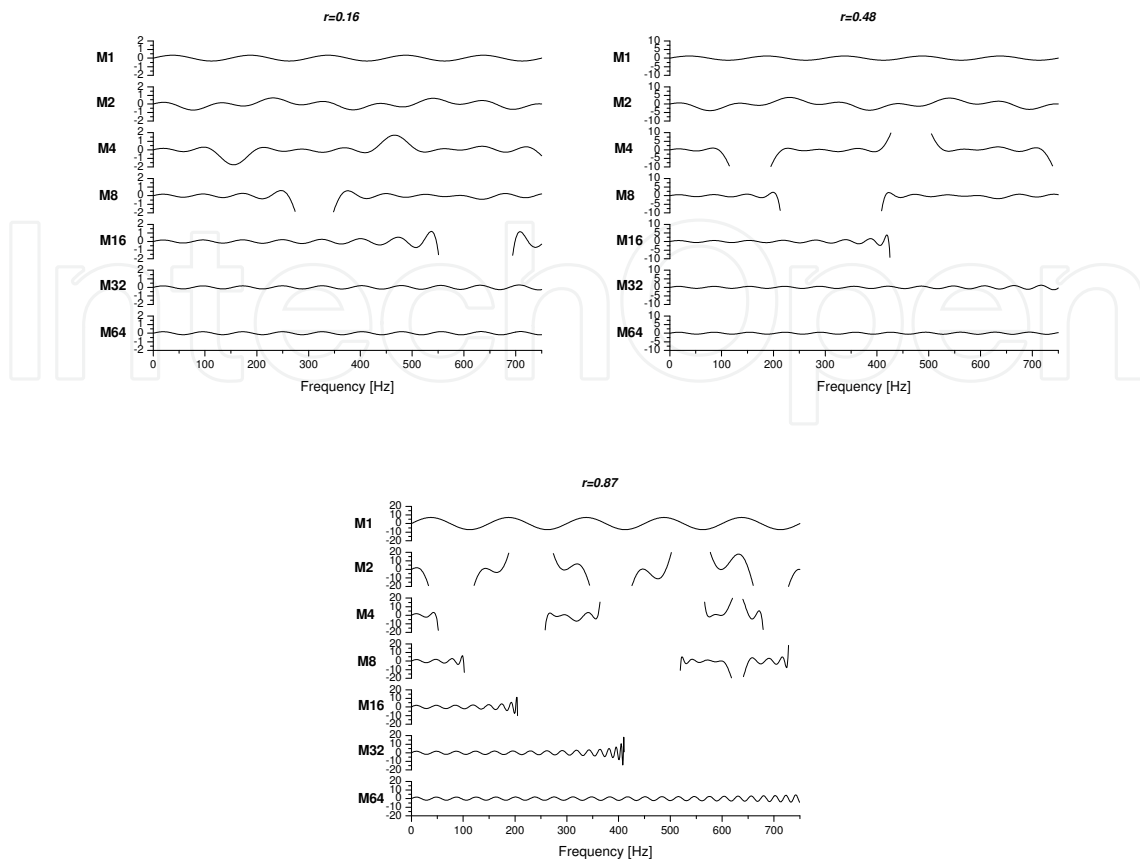


Fig. 15. The amplitude function C (from equation (98)) as a function of frequency (very large values of C are not shown) (Stovas&Ursin, 2007).

coefficient the dampening in transmission amplitudes becomes more dramatic. The exact transmission and reflection responses are computed using a layer recursive algorithm (Ursin and Stovas, 2002). We use a Ricker wavelet with a central frequency of 500 Hz. The transmission and reflection responses are shown in Figure 17 and 18, respectively. No amplitude scaling was used. One can see that these plots are strongly related to the behaviour of $\text{Re } a$ (Figure 13). The upper seismogram in Figure 17 is similar to the Marion and Coudin (1992) experiment and the Hovem (1995) simulations. The effects related to the effective medium (difference between the first arrival traveltimes for model M_1 and M_{64} and the transition between effective and time average medium, models $M_4 - M_{16}$) are the more pronounced for the high reflectivity model. For this model the first two traces (models M_1 and M_2) are composed of separate events, and then the events become more and more interferential as the thickness of the layers decrease. Model M_8 gives trains of nearly sinusoidal waves (tuning effect). The transmission response for model M_{16} is strongly attenuated, and models M_{32} and M_{64} behave as the effective medium. From Figures 13-16 and the transmission and reflection responses (Figures 17 and 18) one can distinguish between time average, effective medium and transition behaviour. This behaviour can be seen for any reflectivity, but a decrease in the reflection coefficient results in the convergence of the traveltimes for time-average and effective medium. This makes the effective medium arrival very close to the time average one. Note also that for the very much-pronounced

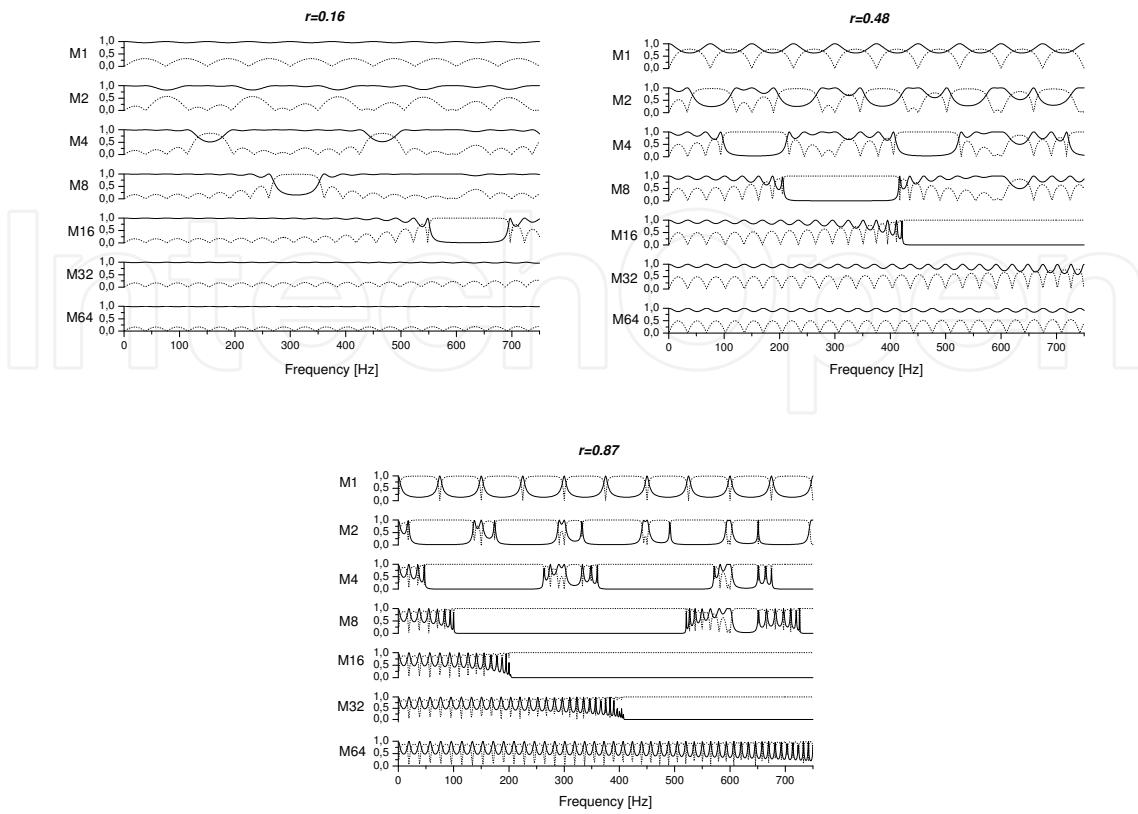


Fig. 16. The transmission amplitude (solid line) and reflection amplitude (dotted line) as function of frequency (Stovas&Ursin, 2007).

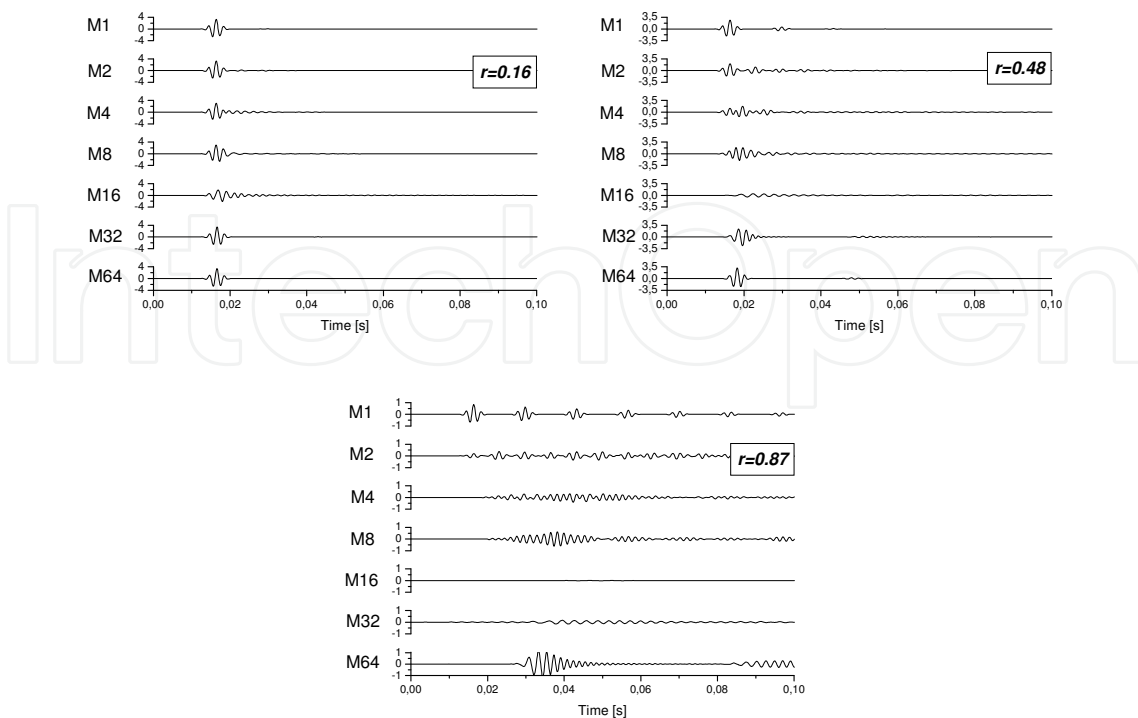


Fig. 17. Numerical simulations of the transmission response (Stovas&Ursin, 2007).

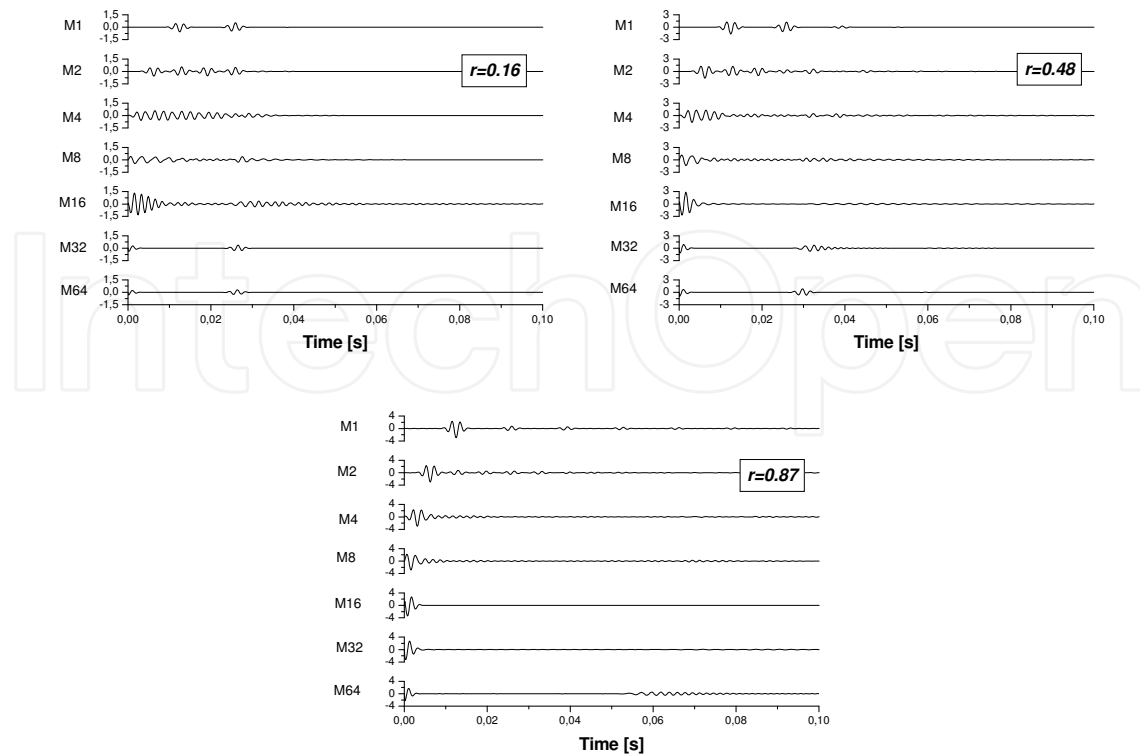


Fig. 18. Numerical simulations of the reflection response (Stovas&Ursin, 2007).

effective medium (model M_{64} , $r = 0.87$) one can see the effective medium multiple on the time about 0.085s. The reflection responses (Figure 18) demonstrate the same features as the transmission responses (for example strongly attenuated transmission response is related to weak attenuated reflection response). Effective medium is represented by the reflections from the bottom of the total stack of the layers. The phase velocities are computed from the phase factor (equation (100)) and shown in Figure 19 as a function of frequency. The phase velocity curve starts from the effective medium velocity and at the critical frequency it jumps up to the time-average velocity. One can see that the width of the transition zone is larger for larger values of reflection coefficient. The difference between the effective medium velocity and time-average velocity limits also increases with reflection coefficient increase.

In Figure 20, one can see time-average velocity, effective medium velocity, phase velocity (equation (100)) and group velocity (equation (102)) computed for reflection coefficients 0.16, 0.48 and 0.87 and model M_{64} . In this case we are in the effective medium zone. The larger reflection coefficient is, the lower effective medium velocity, the larger difference between the phase and group velocity and the velocity dispersion becomes more pronounced. The effective medium velocity limit also depends on the volume fraction ($\phi = h_2 / (h_1 + h_2)$) for one cycle (see equation (104)). This dependence is illustrated in Figure 21 for different values of reflection coefficient. The maximum difference between the time-average and effective medium velocity reaches 2.191 km/s at $\phi = 0.18$ ($r = 0.87$), 0.513 km/s at $\phi = 0.24$ ($r = 0.48$) and 0.053 km/s at $\phi = 0.26$ ($r = 0.16$). One can see that for the small values of reflection coefficient the difference between the time-average velocity (high-frequency limit) and effective medium velocity (low frequency limit) becomes very small. For large values of reflection coefficient and certain range of volume fraction the effective medium velocity is

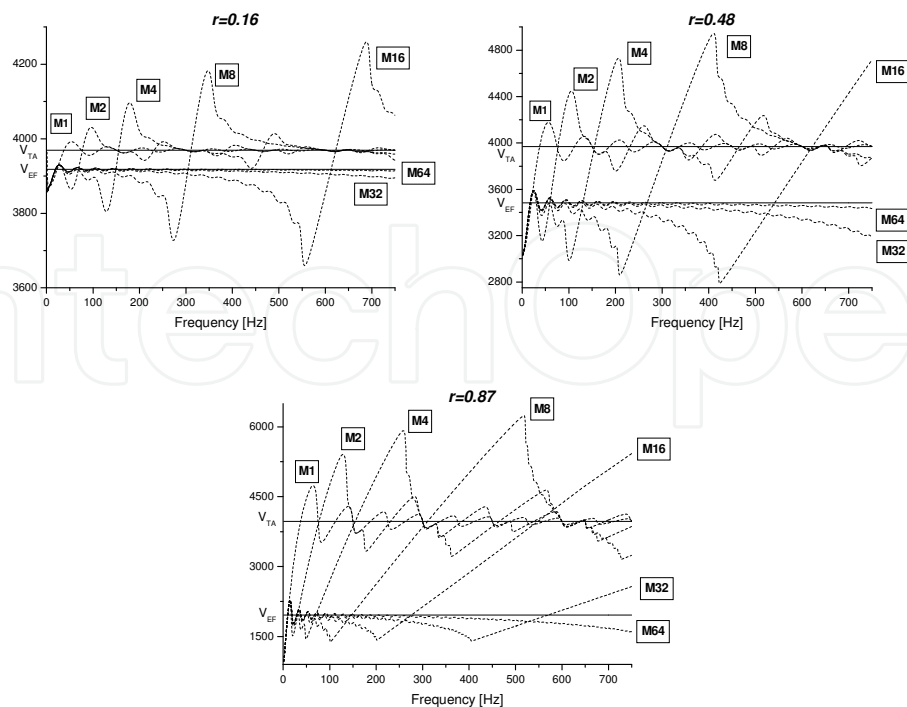


Fig. 19. The phase velocity (equation (101)) in m/s as function of frequency (Stovas&Ursin, 2007).

smaller than the minimum velocity of single layer constitutes. The effective medium is related to the propagating regime. The effective medium velocity depends on the reflection coefficient. The lesser contrast the higher effective medium velocity (the more close to the time-average velocity). One can also distinguish between effective medium, transition and time average frequency bands (Figure 22). These bands are separated by the frequencies given by conditions from the first two roots of equation $\text{Re } a = -1$. The first root (equation (107)) gives the limiting frequency for effective medium. The second one (equation (108)) gives the limiting frequency for time average medium. From Figure 22, one can see that the transition zone converges to the limit $\gamma = 4$ with decreasing reflection coefficient. The first transition zone results in the most significant changes in the phase velocity and the amplitude factor C .

8. High-frequency caustics in periodically layered VTI media

The triplications (caustics) in a VTI medium can also be observed for high-frequencies. They are physically possible for qSV-wave propagation only. The qSV-wave triplications in a homogeneous transversely isotropic medium with vertical symmetry axis (VTI medium) have been discussed by many authors (Dellinger, 1991; Schoenberg and Daley, 2003; Thomsen and Dellinger, 2003; Vavrycuk, 2003; Tygel and et. 2007; Roganov, 2008). The condition for incipient triplication is given in Dellinger (1991) and Thomsen and Dellinger (2003). According to Musgrave (1970), we consider axial (on-axis vertical), basal (on-axis horizontal) and oblique (off-axis) triplications. He also provided the conditions for generation of all the types of triplications. The approximate condition for off-axis triplication is derived in Schoenberg and Daley (2003) and Vavrycuk (2003). The condition for on-axis triplication in multi-layered VTI medium is shown in Tygel et al. (2007).

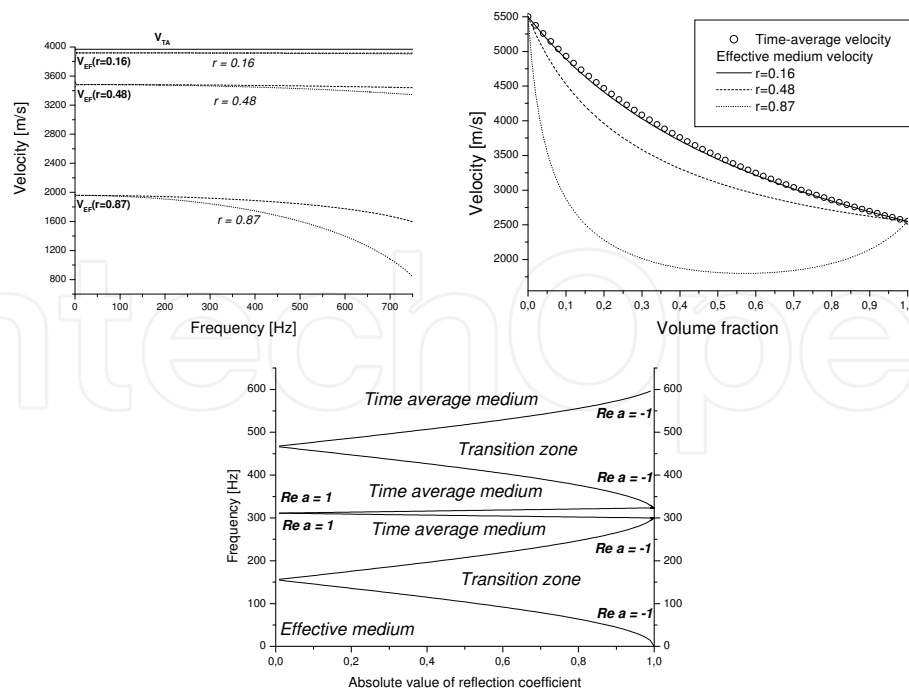


Fig. 20. The time average velocity (equation (105), solid line), the effective medium velocity (equation (104)), the phase velocity (equation (101), dashed line) and the group velocity (equation (102), dotted line) as function of frequency computed for model M_{64} and different reflection coefficients (Stovas&Ursin, 2007) shown to the left. The time-average velocity (equation (105)) and effective medium velocity (equation 104) as a function of volume fraction shown in the middle. Behaviour of the model M_4 as function of frequency and reflection coefficient shown to the right.

8.1 qSV- wave in a homogeneous VTI medium

In a homogeneous anisotropic medium, the plane wave with the slowness surface defined by $q = q(p)$ and the normal (p, q) is given by

$$px + q(p)h = t. \quad (110)$$

The envelope of a family of plane waves given in (110) can be found by differentiation of equation (110) over the horizontal slowness p

$$x + q'(p)h = 0. \quad (111)$$

Equations (110) and (111) define the parametric offset-traveltime equations in a this medium at the depth h and can be written as follows

$$x(p) = -h q', \quad t(p) = -h[pq' - q], \quad (112)$$

where $q' = dq/dp$ is the derivative of vertical slowness. The condition for triplication (caustic in the group space or concavity region on the slowness curve) is given by setting the curvature of the vertical slowness to zero, $q'' = 0$, or by setting the first derivative of offset to zero, $x' = 0$. These points at slowness surface have the curvature equal to zero. If the

triplication region is degenerated to a single point, it is called incipient triplication. At that point we have $q'' = 0$ and $q''' = 0$. For the incipient horizontal on-axis triplication, it is not true, because at that point q' equal to infinity, and we have to take the corresponding limit. The triplications can be also related to the parabolic points on the slowness surface with one of the principal curvatures being zero. The exception is the incipient vertical on-axis triplication with both principal curvatures equal to zero. The phase velocity can be written (Schoenberg and Daley, 2003) as a function of phase angle θ

$$v^2(\theta) = \frac{v_{0s}^2}{2g} f(\theta), \quad (113)$$

where v_{0s} is the vertical S-wave velocity, and function $f(\theta)$ is defined as

$$f(\theta) = f_{p(s)}(\theta) = 1 - eu + g \pm \sqrt{(1 - eu - g)^2 - E(1 - u^2)}, \quad (114)$$

where + and - correspond to qP- and qSV-wave, respectively, $u = \cos 2\theta$, and parameters

$$e = \frac{c_{11} - c_{33}}{c_{11} + c_{33}}, \quad g = \frac{2c_{55}}{c_{11} + c_{33}} \quad \text{and} \quad E = \frac{4(c_{11} - c_{55})(c_{33} - c_{55}) - 4(c_{13} + c_{55})^2}{(c_{11} + c_{33})^2},$$

which can be written in terms of Thomsen (1986) anisotropy parameters

$$e = \varepsilon / (1 + \varepsilon), \quad g = \gamma_0^2 / (1 + \varepsilon), \quad E = 2(\varepsilon - \delta)(1 - e)(1 - e - g) \quad (115)$$

and $\gamma_0 = v_{0s} / v_{0p}$ is the S- to P-wave vertical velocity ratio. Note, that $0 < g < 1$ and $|e| < 1 - g$. Parameter E is also known as anelliptic parameter (Schoenberg and Daley, 2003) since it is proportional to the parameter σ , $\sigma = (\varepsilon - \delta) / \gamma_0^2 = E / (2g(1 - e - g))$, which is responsible for the anellipticity of the slowness surface and for the non-hyperbolicity of the travelttime equation. Vavrycuk (2003) used parameter σ to estimate the critical strength of anisotropy for the off-axis triplications in a homogeneous VTI medium. For the waves propagating for entire range of the phase angles, it is required that the function $f_s(u, E)$ and the expression under the square-root in equation (114)

$$s(u, E) = (1 - eu - g)^2 - E(1 - u^2) \quad (116)$$

should be non-negative for all $|u| \leq 1$. Solving equations $f_s(u, E) = 0$ and $s(u, E) = 0$ for

the parameter E , results in the following explicit functions $E_f(u) = -\frac{4g(1 - eu)}{1 - u^2}$ and

$$E_s(u) = \frac{(1 - eu - g)^2}{1 - u^2},$$

where the sub-indices f and s indicate the solutions for the equations $f = 0$ and $s = 0$, respectively. Function $E_f(u)$ defines the minimum plausible values for the parameter E in order to satisfy the condition $v^2(\theta) \geq 0$, while the function $E_s(u)$ defines the maximum plausible values for the parameter E in order to satisfy the condition $\text{Im } v^2(\theta) = 0$. By setting derivatives $dE_f/du = 0$ and $dE_s/du = 0$, we obtain that,

for the range $|u| < 1$, implicit functions $f_s(u, E) = 0$ and $s(u, E) = 0$ have the maximum and the minimum at the points A_1 (from $f = 0$ and $dE_f/du = 0$) and A_2 (from $s = 0$ and $dE_s/du = 0$), respectively (Figure 21). The coordinates for these points are

$$u_{A_1} = (1 - \sqrt{1 - e^2})/e, \quad E_{A_1} = -2g(1 + \sqrt{1 - e^2}), \quad u_{A_2} = e/(1 - g), \quad E_{A_2} = (1 - g)^2 - e^2. \quad (117)$$

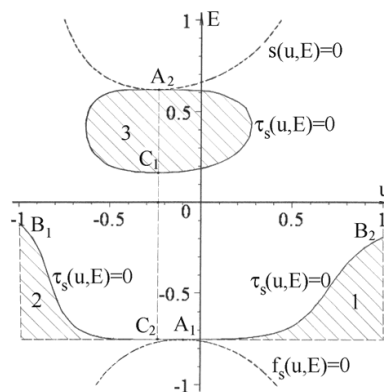


Fig. 21. Schematic plot of the triplication conditions on (u, E) space. The graphs for $f_s(u, E) = 0$ and $s(u, E) = 0$ are shown by dash line, and the graph for $\tau_s(u, E) = 0$ is shown by solid line. Points A_1 and A_2 correspond to the extrema of the functions $f_s(u, E) = 0$ and $s(u, E) = 0$, respectively. Points B_1 and B_2 are the limiting points on the lower branch of $\tau_s(u, E) = 0$ from the left and from right, respectively. Points A_2 , C_1 and C_2 correspond to the extrema of the function $\tau_s(u, E) = 0$ which has two branches limiting the triplication areas: 1 - vertical on-axis, 2 - horizontal on-axis and 3 - off-axis. The condition $E_{A_1} \leq E \leq E_{A_2}$ is a necessary and sufficient condition for existence of qP- and qSV-waves for entire range of the phase angles (Roganov&Stovas, 2010).

Therefore, the parameter E is limited as follows $E_{A_1} \leq E \leq E_{A_2}$. Note, that $u_{A_1} = 0$ if $e = 0$. The equation for u_{A_2} was shown in Schoenberg and Daley (2003). The lower limit yields the condition $v^2(\theta) \geq 0$, while the upper limit is related to the Thomsen's (1986) definition of parameter δ , i.e. $1 + 2\delta - \gamma_0^2 \geq 0$. The range for parameter E yields a necessary and sufficient condition for the Christoffel matrix being positive definite for the entire range of the phase angles. Therefore, this condition is valid for all physically plausible medium parameters. Using equation (113) and

$$p = \sin \theta / V(\theta), \quad q = \cos \theta / V(\theta), \quad u = \cos 2\theta,$$

we obtain that for both types of waves we have the following equalities p

$$p = \frac{1}{v_{os}} \sqrt{\frac{(1-u)g}{f}}, \quad q = \frac{1}{v_{os}} \sqrt{\frac{(1+u)g}{f}}, \quad (118)$$

where $f = f_{p(s)}$ depending on the wave-mode (see equation (114)). The first and second derivatives of the vertical slowness are given by

$$\frac{dq}{dp} = \frac{p(-f + f'_u \cdot (1+u))}{q(f + f'_u \cdot (1-u))}, \quad (119)$$

$$\frac{d^2q}{dp^2} = \frac{2\tau g}{v_{0s}^2 q^3 \chi^3}, \quad (120)$$

where $f'_u = df/du$ and

$$\chi = \chi_{p(s)} = (1-e-g)(1-eu-g) - E(1-u) \pm (1-e+g)\sqrt{s}, \quad \tau = \tau_{p(s)} = m \mp n\sqrt{s} \quad (121)$$

with s given in equation (116) and

$$m = 2E[-e(e^2 - 2g + 2g^2)u^3 + 3e^2(1-g)u^2 - 3e(1-g^2)u + (1+g)(1-g)^2 + 2e^2g] - 2(1-e^2-g^2)(1-eu-g)^3. \quad (122)$$

$$n = -(1-u^2)E^2 - [(1+e^2+g^2-6g)u^2 - 4e(1-g)u + e^2 + (1+g)^2]E + 2(1+g^2-e^2)(1-eu-g)^2$$

For qSV and qP waves propagating in a homogeneous VTI medium, the triplication condition is given by (Roganov, 2008)

$$\tau_s(u, E) = 0, \quad (123)$$

$$\tau_p(u, E) = 0. \quad (124)$$

Equations (121)-(122) are too complicated to define the influence of parameters e and g on the form of the curves given by equations (123) and (124). Nevertheless, these equations can be used for numerical estimation of the position for triplications with any given values for e and g , as well as for the following theoretical analysis. It is well known that qP waves never have triplications in a homogeneous VTI medium (Musgrave, 1970; Dellinger, 1991; Vavrycuk, 2003), and, therefore, the equation (124) has no roots for propagating qP waves. By taking all the physically possible values for u , e , g and E , one can prove that if $s(u, E) \geq 0$, $|u| \leq 1$, $0 < g < 1$ and $|e| < 1 - g$, the following inequality always takes place, $\tau_p(u, E) < 0$.

The product of $\tau_p(u, E)$ and $\tau_s(u, E)$

$$\tau(u, E) = \tau_p(u, E)\tau_s(u, E) = m^2 - sn^2 \quad (125)$$

given by polynomial with the sixth order in u and fifth order in E , can also be used to define the triplications for qSV-waves. For elliptical anisotropy, $E = 0$, we have the equalities $f_s(u, E) \equiv 2g$ and $V^2(\theta) \equiv c_{55}$. In this case, both the slowness and the group velocity surfaces are circles, and qSV-waves have no triplications. The straight line given by $E = 0$, separate the plane (u, E) into sub-planes with non-crossing branches of the curve $\tau_s(u, E) = 0$. One of these branches is located in the range of values $E_{A1} < E < 0$ and $|u| \leq 1$ and is limited from the left and the right by the points B_1 and B_2 , respectively. The coordinates of these points are (Figure 23)

$$u_{B_1} = -1, \quad E_{B_1} = -g(1+e-g), \quad u_{B_2} = 1, \quad E_{B_2} = -g(1-e-g), \quad (126)$$

while the second branch is closed and located in the range of values $0 < E < E_{A_2}$. The limited values $E_{B_1} < 0$ and $E_{B_2} < 0$, that follows from inequalities $0 < g < 1$ and $|e| < 1 - g$. Under the lower branch of the curve $\tau_s(u, E) = 0$ on the plane (u, E) , there are two parameter areas resulting in the on-axis triplications (both for vertical and horizontal axis), while the upper branch of the curve $\tau_s(u, E) = 0$ defines the parameter area for the off-axis triplications. In Figure 23, these areas are denoted by numbers 1, 2 and 3, respectively. Therefore, the on-axis triplications can simultaneously happen for both axis, if $E < 0$, while the off-axis triplications can exist only alone, if $E > 0$. Let us define the critical values for parameter E in (u, E) space with horizontal tangent line (E_{A_1} , E_{A_2} , E_{C_1} and E_{C_2} in Figure 23) that define the incipient triplications. In order to do so we need to solve the system of equations

$$\begin{cases} \tau_s(u, E) = 0 \\ \frac{\partial \tau_s(u, E)}{\partial u} = 0 \end{cases}. \quad (127)$$

For the range of parameters $E_{A_1} \leq E \leq E_{A_2}$ and $|u| \leq 1$, system of equations (127) has four solutions, where the first two solutions $\{u_{A_1}, E_{A_1}\}$ and $\{u_{A_2}, E_{A_2}\}$ are defined above. For the second two solutions $\{u_{C_1}, E_{C_1}\}$ and $\{u_{C_2}, E_{C_2}\}$ we have $u_{C_1} = u_{C_2} = u_{A_2}$, while E_{C_1} and E_{C_2} are the largest (always positive) and intermediate (always negative) roots of the cubic equation

$$t(E) = E^3 + (3g^2 - 3e^2 + 2g + 3)E^2 + 8g(1 + g^2 - e^2)E - 16g^2(1 - e^2) \left((1 - g)^2 - e^2 \right) = 0. \quad (128)$$

Equations similar to our equation (128) are derived in (Peyton, 1983; Schoenberg and Helbig, 1997; Thomsen and Dellinger, 2003; Vavrycuk, 2003; Roganov, 2008). To prove that equation $t(E) = 0$ gives the positions for the critical points of the curve $\tau(u, E) = 0$ one can substitute $u = u_{A_2}$. Consequently, we have

$$\tau(u_{A_2}, E) = \frac{\left((1 - g)^2 - e^2 \right)}{(1 - g)^2} t(E) p^2(u_{A_2}, E) \quad (129)$$

and

$$\frac{\partial \tau(u_{A_2}, E)}{\partial u} = \frac{6e(1 - g)}{(1 - g)^2 - e^2} \tau(u_{A_2}, E). \quad (130)$$

Therefore, if $t(E) = 0$ and $u = u_{A_2}$, then system of equations (127) is obeyed. The least root of equation (128) is located in the area defined by $E < -1$ and holds also equation $\tau_p(u, E) = 0$. It is located outside the region $E_{A_1} \leq E \leq E_{A_2}$ and does not define any qSV wave triplication. The intermediate root defines the critical point C_2 on the lower branch of the curve (123). The minimum point A_1 (dividing the triplication domain 1 and 2) is also

located on the same branch. The largest root corresponds to the minimum point C_1 on the upper branch of the curve (123). If $E_{c1} < E < E_{A1}$, we have off-axis triplications. The coordinates E_{c1} and E_{c2} are given by equations

$$E_{c1} = 2Q \sin(2\psi / 3 + \pi / 6) - d, \quad E_{c2} = 2Q \sin(2\psi / 3 + 5\pi / 6) - d, \quad (131)$$

where

$$d = 1 + 2g / 3 + g^2 - e^2, \quad Q = |1 - e^2 - 2g / 3 + g^2|, \quad \psi = \arccos \frac{\sqrt{[(1-g)^2 - e^2](1 - e^2 - g^2)}}{Q^{3/2}}. \quad (132)$$

The case for the qSV-wave vertical on-axis incipient triplication can be obtained by setting $u = 1$ ($\theta = 0$) with condition (120) being simplified to $E = E_{B2}$ or $\sigma = -0.5$ or $v_{nmo}^2 = 0$ (Tygel et al., 2007). The case for the qSV-wave horizontal on-axis incipient triplication can be obtained by setting $u = -1$ ($\theta = \pi/2$) with condition (118) being simplified to $E = E_{B1}$ or $\sigma = -(1 + 2\varepsilon - \gamma_0^2) / 2(1 - \gamma_0^2)$. If $E_{A1} < E < \min(E_{B1}, E_{B2})$, we have both on-axis triplications. If $e = 0$ (or $\varepsilon = 0$), then we have the following equality $E_{B1} = E_{B2}$, and, therefore, both on-axis triplications are incipient.

8.2 Extension of qSV-wave triplications for multilayered case

From the ray theory it follows that for any vertically heterogeneous medium including horizontally layered medium, kinematically effective vertical slowness is always the average of the vertical slownesses from the individual layers. We have to stress that our approach is based on the high-frequency limit of the wave propagation, not on the low-frequency one which results in effective medium averaging. Since the wave propagates through the layered medium with the same horizontal slowness p , the effective vertical slowness has very simple form

$$\tilde{q} = \langle q \rangle, \quad (133)$$

where $\langle \rangle$ denotes the arithmetic thickness averaging, $\langle m \rangle = \sum m_i h_i / \sum h_i$, with $h_i, i = 1, N$ being the thickness of layer i in the stack of N layers. With notation (133), equations (112) are valid for the multilayered case. Similar approach is used in Stovas (2009) for a vertically heterogeneous isotropic medium. If a layered VTI medium results in more than one caustic, there is no any kinematically effective VTI medium given in equation (133), which can reproduce the same number of caustics. This statement follows from the fact that a homogeneous VTI medium might have only one off-axis triplication. Therefore, the second derivative of the effective vertical slowness is given by

$$\frac{d^2 \tilde{q}}{dp^2} = \left\langle \frac{2\tau g}{v_{0s}^2 q^3 \chi^3} \right\rangle. \quad (134)$$

With equation (134) the condition for off-axis, vertical on-axis and horizontal on-axis triplications in multi-layered VTI medium takes the form (Roganov and Stovas, 2010)

$$\left\langle \frac{\tau_s g}{v_{0s}^2 q_s^3 \chi_s^3} \right\rangle = 0. \quad (135)$$

To obtain the condition for incipient vertical triplications, we have to substitute $u = 1$ и $p = 0$ into equation (135). After some algebraic manipulations, we obtain

$$\left. \frac{d^2 \tilde{q}}{dp^2} \right|_{u=1, p=0} = - \left\langle \frac{v_{0s} (E_{B2} - E)}{E_{B2}} \right\rangle = 0. \quad (136)$$

Similar equation can be derived by using the travelttime parameters. Tygel et al. (2007) shown that the vertical on-axis triplications in the multilayered VTI medium are defined by the normal moveout velocity (representing the curvature of the travelttime curve $t(x)$ taken at zero offset): $\tilde{v}_{nmo}^2 = 0$, where $\tilde{v}_{nmo}^2 = \langle v_{nmo}^2 v_{0s}^{-1} \rangle / \langle v_{0s}^{-1} \rangle$ is the overall normal moveout velocity squared. In order to use equation (135), the function $u(p)$ has to be defined in terms of horizontal slowness for each layer

$$u(p) = u_s(p) = \frac{a + p^2 v_{0s}^2 \sqrt{b}}{c}, \quad (137)$$

where

$$\begin{aligned} a &= g^2 - g(1+e+g)p^2 v_{0s}^2 + 2egp^4 v_{0s}^4 \\ b &= g^2(1-e-g)^2 + 2g[2eg(1-e-g) - (1-e+g)E]p^2 v_{0s}^2 + (E^2 + 4Eg + 4e^2 g^2)p^4 v_{0s}^4. \\ c &= g^2 - 2egp^2 v_{0s}^2 - Ep^4 v_{0s}^4 \end{aligned} \quad (138)$$

Function $b(p) > 0$ if $E > 0$. We are going to prove that the function $b = b(p)$ from equation (138) is positive for all physically plausible parameters e and g , if anelliptic parameter $E > 0$. Solving bi-quadratic equation $b(p) = 0$ yields

$$p_{1,2,3,4} = \pm \frac{1}{v_{0s}} \sqrt{\frac{Eg(1-e+g) - 2eg^2(1-e-g) \pm 2\sqrt{E(1-e)(e^2 + E - (1-g)^2)}}{E^2 + 4Eg + 4e^2 g^2}} \quad (139)$$

The expression under the inner square root in equation (139) can be written as

$$e^2 + E - (1-g)^2 = -4(1-\gamma_0^2)(1+2\delta - \gamma_0^2) \quad (140)$$

Note, that $1+2\delta - \gamma_0^2 \geq 0$ (it follows from Thomsen's (1986) definition of parameter δ). Taking into account that $e < 1$, and $b(p=0) = g^2(1-e-g)^2 > 0$ and $b(p=1/v_{0s}) = (1-e)^2(1+e-g)^2 > 0$, one can see that if $E > 0$, the expression under the square root in equation (139) is negative, and the equation $b(p) = 0$ has no roots. Function $c = c(p)$ can take zero value at

$$p = \tilde{p} = \pm \frac{1}{v_{0s}} \sqrt{\frac{g}{E} \left(-e + \sqrt{e^2 + E} \right)} \quad (141)$$

To compute $u = u(\tilde{p})$ from equation (137) we need to take the limit given by

$$\lim_{p \rightarrow \tilde{p}} u(p) = u(\tilde{p}) = \frac{4e^2g + E(e + e^2 + 2g + eg) + E^2 - \sqrt{e^2 + E}(4eg + E(1 + e + g))}{4e^3g + E(e + e^2 + 3eg) + E^2 - \sqrt{e^2 + E}(4e^2g + E(1 + e + g))}. \quad (141)$$

If $c(p) = 0$, that happens at

$$p = \tilde{p} = \frac{1}{v_{0s}} \sqrt{\frac{g}{E} \left(-e + \sqrt{e^2 + E} \right)}, \quad (142)$$

function $u(p)$ takes the value

$$u(\tilde{p}) = \frac{4e^2g + E(e + e^2 + 2g + eg) + E^2 - \sqrt{e^2 + E}(4eg + E(1 + e + g))}{4e^3g + E(e + e^2 + 3eg) + E^2 - \sqrt{e^2 + E}(4e^2g + E(1 + e + g))}. \quad (143)$$

Note that in the presence of on-axis triplication (for the horizontal axis), function $u(p)$ has two branches when $|p| > 1/v_{s0}$, and the second branch is defined by $u(p) = u_p(p) = (a - p^2 v_{0s}^2 \sqrt{b})/c$. The incipient off-axis triplication condition in a multilayered medium is given by equation (Roganov and Stovas, 2010)

$$\left\langle \frac{g}{v_{0s}} \frac{d \left(\frac{\tau_s}{q_s^3 \chi_s^3} \right)}{dp} \right\rangle = 0. \quad (144)$$

Functions q_s and τ_s, χ_s defined in equations (118) and (121), respectively, are given in terms of u . To compute the derivatives in equation above one need to exploit equation (117) for $u = u(p)$ and apply the chain rule, i.e. $dq_s/dp = (dq_s/du)(du/dp)$. For a given model this equation can be resolved for horizontal slowness and used to estimate the limits for the vertical slowness approximation or travelttime approximation. For multilayered case, the parametric offset-traveltime equations (112) take the following form

$$\tilde{x}(p) = -H \tilde{q}', \quad \tilde{t}(p) = -H [p\tilde{q}' - \tilde{q}], \quad (145)$$

where $H = \sum h_i$ is the total thickness of the stack of layers.

8.3 Converted wave case

In the special case of converted qP-qSV waves (C-waves) in a homogeneous VTI medium, the condition (113) reduces to

$$\frac{\tau_s}{q_s^3 \chi_s^3} + \frac{\tau_p}{q_p^3 \chi_p^3} = 0. \quad (146)$$

To compute functions τ_p , q_p and χ_p we need to define $u_p(p)$ which can be computed similar to equation (117)

$$u_p(p) = \frac{a - p^2 v_{0s}^2 \sqrt{b}}{c}, \quad (147)$$

where functions a , b and c can be computed from equation (138). One can show that for the range of horizontal slowness corresponding to propagating qP-wave, the sum

$$\frac{\tau_s}{q_s^3 \chi_s^3} + \frac{\tau_p}{q_p^3 \chi_p^3} < 0, \quad (148)$$

which means that the converted qP-qSV waves in a homogeneous VTI medium have no triplications. In Figure 22 one can see the functions $2\tau_s/q_s^3 \chi_s^3$ (controlling the triplications for qSV-wave), $2\tau_p/q_p^3 \chi_p^3$ (controlling the triplications for qP-wave) and $\tau_s/q_s^3 \chi_s^3 + \tau_p/q_p^3 \chi_p^3$ (controlling the triplications for converted waves). The model parameters are taken from the case 1 model 1. One can see that the only function crossing the u -axis is the qSV-wave related one.

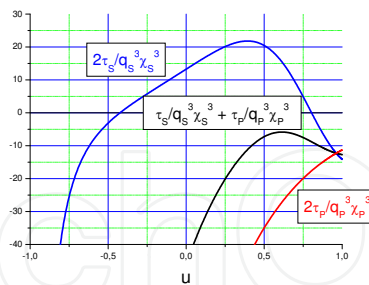


Fig. 22. The functions controlled the qP- (red line), qSV- (blue line) and qPqSV-wave (black line) triplications. The data are taken from the case 1 model 1 (Roganov&Stovas, 2010).

8.4 Single-layer caustics versus multi-layer caustics

For our numerical tests we consider the off-axis triplications only, because the vertical on-axis triplications were discussed in details in Tygel et. al (2007), while the horizontal on-axis triplications have only theoretical implications.

First we illustrate the transition from the vertical on-axis triplication to the off-axis triplication by changing the values for parameter E only, $E = -0.3, -0.2, \dots, 0.5$. Since the other parameters remain constant, this change corresponds to the changing in Thomsen's

(1986) parameter δ . The slowness surfaces, the curvature of the slowness surfaces and the traveltime curves are shown in Figure 23. One can see how the anomaly in the curvature moves from zero slowness to non-zero one.

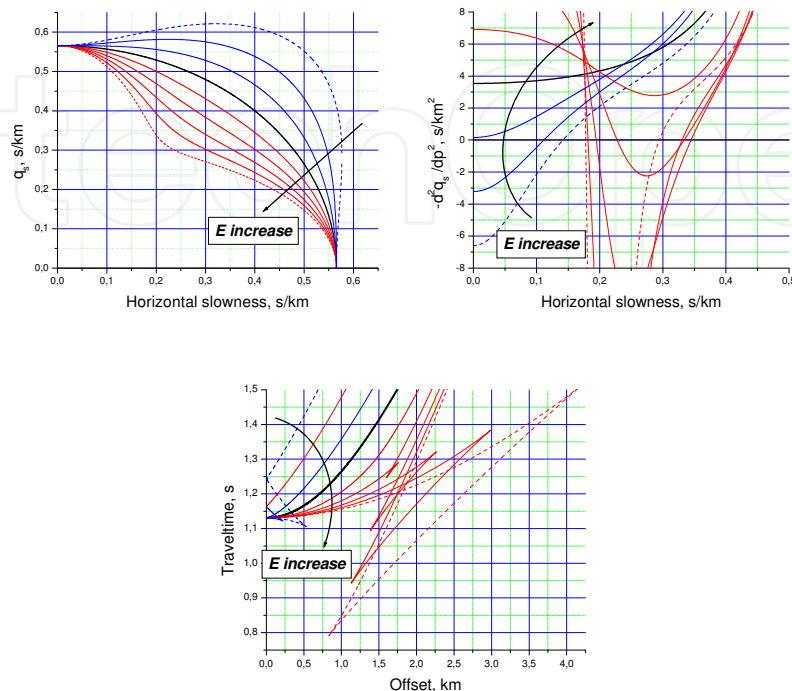


Fig. 23. The slowness surface (to the left), the curvature of slowness surface (in the middle) and the traveltime versus offset (to the right) from the homogeneous VTI media with change in parameter E only. The model parameters are taken from the model 1 in Table 1.

Parameter E takes the values $-0.3, -0.2, \dots, 0.5$. The curves with positive and negative values for E are shown with red lines and blue lines, respectively. The elliptically isotropic case, $E = 0$, is shown by black line (Roganov&Stovas, 2010).

Next we test the qSV-wave slowness-surface approximations from Stovas and Roganov (2009). The slowness-surface approximations for qSV waves (similar to acoustic approximation for qP waves) are used for processing (in particular, phase-shift migration) and modeling purpose with reduced number of medium parameters. With that respect, it is important to know how the slowness-surface approximations reproduce the triplications. We notice that if the triplication is located for short offset, it can partly be shown up by approximation 1 (short spread approximation). The wide-angle approximations 2 and 3 can not treat the triplications.

In the numerical examples provided in Roganov and Stovas (2010), we considered four cases with two layer models when each layer has parameters resulting in triplication for qSV-wave. With changing the fraction ratio from 0 to 1 with the step of 0.1, we can see the transition between two different triplications for cases 1-4. For given numbers of the fraction ratio we can observe the different cases for two-layer triplications. For the overall propagation we can have no triplication (case 1), one triplication (case 2), two triplications (case 3) and one "pentaplication" or two overlapped triplications (case 4). Intuitively, we can say that the most complicated caustic from N VTI layers can be composed from N

overlapped triplications or one “(2N+1)-plication”. The examples shown in Roganov and Stovas (2010) provide the complete set of situations for off-axis triplications in two-layer VTI media and give a clue what we can expect to see from multilayered VTI media.

9. Phase velocity approximation in finely layered sediments

The effect of multiple scattering in finely layered sediments is of importance for stratigraphic interpretation, matching of well log-data with seismic data and seismic modelling. This problem was first studied in the now classical paper by O'Doherty and Anstey (1971) and further investigated by Shapiro and Treitel (1997). In this paper I derive a new approximation for the phase velocity in an effective medium which depends on three parameters only and show how it depends on the strength of the reflection coefficients (Stovas, 2007). Approximation is tested on the real well log data example and shows very good performance.

9.1 Vertical propagation through the stack of the layers

The transmission and reflection responses of normal-incident plane wave from the stack of N layers are given by the following expressions (Stovas and Arntsen, 2006)

$$t_d^{(N)} = \frac{e^{i\vartheta_N} \prod_{k=1}^N (1-r_k)}{[1+\Phi]}, \quad r_d^{(N)} = \frac{e^{2i\vartheta_N} \left(\sum_{j=1}^N r_j e^{-2i(\vartheta_N - \vartheta_j)} + \dots \right)}{[1+\Phi]}, \quad (149)$$

where r_k are reflection coefficients, the cumulated phases $\vartheta_i = \omega \sum_{i=1}^N \tau_i = \omega \sum_{i=1}^N h_i / V_i$, with h_j

and V_j are thickness and velocity in the layer j , respectively, and the reflection coefficient correlation function

$$\Phi = \sum_{k=1}^{N-1} \sum_{j=k+1}^N r_k r_j e^{2i(\vartheta_j - \vartheta_k)} + \dots \quad (150)$$

The exponential factors in denominators for transmission and reflection response are the phase delays for direct wave, the product function in transmission response gives the direct transmission loss and the sum function in reflection response corresponds to contributions from the primary reflections (first order term) and interbedded multiples (higher order terms).

The phase velocity is given by

$$\frac{1}{V(\omega)} = \frac{1}{V_{TA}} - \frac{1}{\omega D} a \tan \frac{\text{Im } \Phi}{1 + \text{Re } \Phi} = \frac{1}{V_{TA}} - \frac{1}{\omega D} a \tan \frac{\sum_{k=1}^{N-1} \sum_{j=k+1}^N r_k r_j \sin 2(\vartheta_j - \vartheta_k) + \dots}{1 + \sum_{k=1}^{N-1} \sum_{j=k+1}^N r_k r_j \cos 2(\vartheta_j - \vartheta_k) + \dots}, \quad (151)$$

where D is the total thickness of the stack and $V_{TA} = \omega D / \vartheta_N$ is time-average velocity. The velocity in zero-frequency limit is given by (Stovas and Arntsen, 2006)

$$\frac{1}{V_0} = \lim_{\omega \rightarrow 0} \frac{1}{V(\omega)} = \frac{1}{V_{TA}} - \frac{2}{D} \frac{\sum_{k=1}^{N-1} \sum_{j=k+1}^N r_k r_j (\tau_j - \tau_k) + \dots}{1 + \sum_{k=1}^{N-1} \sum_{j=k+1}^N r_k r_j + \dots} \quad (152)$$

9.2 Weak-contrast approximation

The weak-contrast approximation means that we neglect the higher order terms in the scattering function Φ (equation 150),

$$\Phi = \sum_{k=1}^{N-1} \sum_{j=k+1}^N r_k r_j e^{2i(\vartheta_j - \vartheta_k)} \quad (153)$$

This function can be expanded into Taylor series

$$\Phi = \sum_{n=0}^{\infty} \frac{(2i\omega)^n}{n!} u_n \quad (154)$$

with coefficients

$$u_n = \sum_{k=1}^{N-1} \sum_{j=k+1}^N r_k r_j (\tau_j - \tau_k)^n \quad (155)$$

which can be considered as correlation moments for reflection coefficients series. To approximate equation (155) we use

$$u_n = u_0 \tau_N^n e^{-\alpha n}, \quad n = 0, 1, 2, \dots, \quad (156)$$

where $\tau_N = \vartheta_N / \omega$ is total one-way propagation time and parameter α will be explained later. The form of approximation (156) has been chosen due to the exponential nature of the reflection coefficient correlation moments (O'Doherty and Anstey, 1971), and the term τ_N^n is introduced simply to preserve the dimension for u_n . Substituting (156) into (154) results in

$$\Phi = u_0 \sum_{n=0}^{\infty} \frac{(2i\omega\tau_N)^n}{n!} e^{-\alpha n} \quad (157)$$

Equation (151) in weak contrast approximation is reduced to (Stovas, 2007)

$$\frac{1}{V(\omega)} = \frac{1}{V_{TA}} - \frac{1}{\omega D} \text{Im} \Phi = \frac{1}{V_{TA}} [1 - \beta(1 + S(\omega))] \quad (158)$$

with $\beta = 2u_0 e^{-\alpha} = 2u_1 / \tau_N$ and $S(\omega) = \sum_{n=1}^{\infty} \frac{(-1)^n (2\omega\tau_N)^{2n}}{(2n+1)!} e^{-2n\alpha}$, where u_0 being considered

as the zero-order auto-correlation moment for reflection coefficients series

$u_0 = \sum_{k=1}^{N-1} \sum_{j=k+1}^N r_k r_j$ and α is the parameter in correlation moments approximation. For practical

use we need the limited number of terms M in equation (160). The zero-frequency limit from equation (152) is given by $V_0^{-1} = V_{TA}^{-1} - 2u_1 / D = (1 - \beta) / V_{TA}$. Substituting this limit into equation (158) we obtain

$$\frac{1}{V(\omega)} = \frac{1}{V_0} \left[1 - \frac{\beta}{1 - \beta} S(\omega) \right]. \quad (163)$$

Parameter $\beta \leq 0$, therefore, describes the relation between two limits $\beta = 1 - V_{TA} / V_0$ and function $S(\omega)$ can be interpreted as the normalized relative change in the phase slowness $-S(\omega) = (V_0^{-1} - V^{-1}) / (V_0^{-1} - V_{TA}^{-1})$.

The phase velocity approximation is described by three parameters only: one-way propagation time τ_N ; 2) parameter β which is ratio of low and high frequency velocity limits; 3) parameter α which describes the structure of the stack.

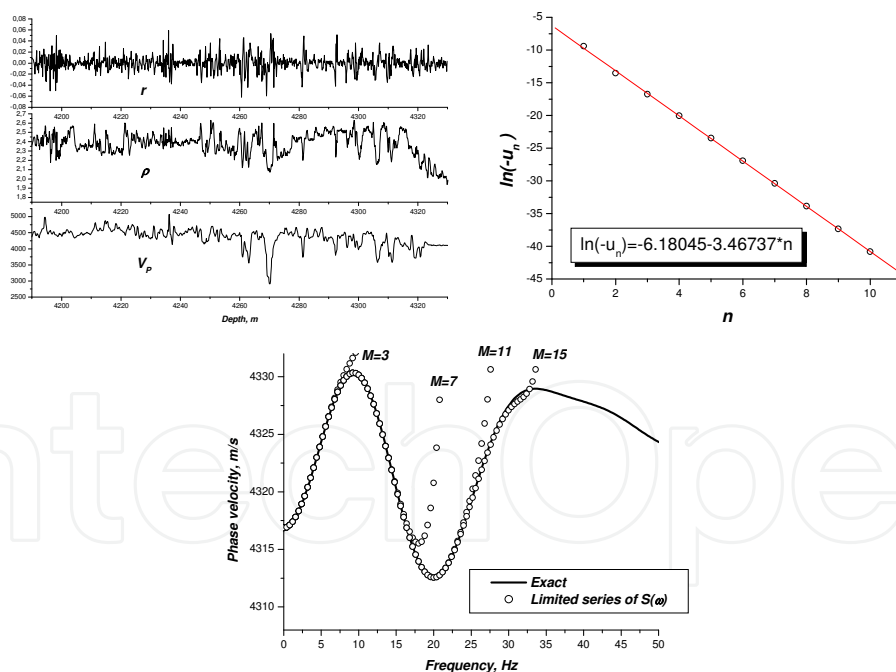


Fig. 24. Elastic parameters and reflection coefficients for Tilje formation (to the left), the correlation moments approximation (in the middle) and the phase velocity and its approximations computed from limited series of $S(\omega)$. (Stovas, 2007).

For numerical application we use 140m of the real well-log data sampled in 0.125m (Figure 24). This interval related to the Tilje formation from the North Sea. In Figure 24, we also show how to compute parameters for approximation (156). The one way traveltime is

$\tau_N = 0.0323 s$, $\beta = -0.04$ and $\alpha = 0.03468$. In particular it means that the time-average velocity is only 4% higher than the zero frequency limit. The results of using this approximation with the limited number of terms ($M = 3, 7, 11$ and 15) in equation (157) are shown in Figure 24. The exact phase velocity function is obtained from the transmission response computed by the matrix propagator method (Stovas and Arntsen, 2006). One can see that with increase of M the quality of approximation increases with frequency.

10. Estimation of fluid saturation in finely layered reservoir

The theory of reflection and transmission response from a stack of periodically layered sediments can be used for inversion of seismic data in turbidite reservoirs. In this case, the model consists of sand and shale layers with quasi-periodical structure. The key parameters we invert for are the net-to-gross ratio (the fractural amount of sand) and the fluid saturation in sand. The seismic data are decomposed into the AVO (amplitude versus offset) or AVA (amplitude versus incident angle) attributes. The following notations are used: AVO intercept is the normal reflectivity and AVO gradient is the first order term in Taylor series expansion of reflectivity with respect to sine squared of incident angle.

For simultaneous estimation of net-to-gross and fluid saturation we can use the PP AVO parameters (Stovas, Landro and Avseth, 2006). To model the effect of water saturation we use the Gassmann model (Gassmann, 1951). Another way of doing that is to apply the poroelastic Backus averaging based on the Biot model (Gelinsky and Shapiro, 1997). Both net-to-gross and water saturation can be estimated from the cross-plot of AVO parameters. This method is applied on the seismic data set from offshore Brazil. To build the AVO cross-plot for the interface between the overlaying shale and the turbidite channel we used the rock physics data. These data were estimated from well logs. The AVO cross-plot contains the contour lines for intercept and gradient plotted versus net-to-gross and water saturation. The discrimination between the AVO attributes depends on the discrimination angle (angle between the contour lines, see Stovas and Landrø, 2004). One can see that the best discrimination is observed for high values of net-to-gross and water saturation, while the worst discrimination is for low net-to-gross and water saturation (where the contour lines are almost parallel each other). Note, that the inversion is performed in the diagonal band of AVO attributes. Zones outside from this band relate to the values which are outside the chosen sand/shale model. Our idea is that the top reservoir reflection should give relatively high values for net-to-gross regardless to water saturation values. The arbitrary reflection should give either low values for net-to-gross with large uncertainties in water saturation or both net-to-gross and saturation values outside the range for the chosen model. The data outside the diagonal band are considered as a noise. To calibrate them we use well-log data from the well. The P-wave velocity, density and gamma ray logs are taken from the well-log. One can say that the variations in the sand properties are higher than we tested in the randomization model. Nevertheless, the range of variations affects more on the applicability of the Backus averaging (which is weak contrast approximation) than the value for the Backus statistics. The AVO attributes were picked from the AVO sections (intercept and gradient), calibrated to the well logs and then placed on the cross-plot. One might therefore argue that the AVO-attributes themselves can be used as a hydrocarbon indicator, and this is of course being used by the industry. However, the attractiveness of the proposed method is that we convert the two AVO-attributes directly into net-to-gross and saturation

attributes, in a fully deterministic way. Furthermore the results are quantitative, given the limitations and simplifications in the model being used.

11. Seismic attributes from ultra-thin reservoir

Here we propose the method of computation seismic AVO attributes (intercept and gradient) from ultra-thin geological model based on the SBED modelling software (Stovas, Landro and Janbo, 2007). The SBED software is based on manipulating sine-functions, creating surfaces representing incremental sedimentation. Displacement of the surfaces creates a three dimensional image mimicking bedform migration, and depositional environments as diverse as tidal channels and mass flows can be accurately recreated. The resulting modelled deposit volume may be populated with petrophysical information, creating intrinsic properties such as porosity and permeability (both vertical and horizontal). The Backus averaging technique is used for up-scaling within the centimetre scale (the intrinsic net-to-gross value controls the acoustic properties of the ultra-thin layers). It results in pseudo-log data including the intrinsic anisotropy parameters. The synthetic seismic modelling is given by the matrix propagator method allows us to take into account all pure mode multiples, and resulting AVO attributes become frequency dependent. Within this ultra-thin model we can test different fluid saturation scenarios and quantify the likelihood of possible composite analogues. This modelling can also be used for inversion of real seismic data into net-to-gross and fluid saturation for ultra-thin reservoirs.

11.1 SBED model

The SBED software is based on manipulating sine-functions, creating surfaces representing incremental sedimentation (Wen, 2004; Nordahl, 2005). Displacement of the surfaces creates a three-dimensional image mimicking bedform migration, and depositional environments as diverse as tidal channels and mass flows can be accurately recreated. Due to the high-resolution output, common practice is to generate models that are volumetrically slightly larger than real core data (30 x 30 cm in x and y directions). The resulting modelled deposit volume may be populated with petrophysical information, creating intrinsic properties such as porosity and permeability (both vertical and horizontal). These petrophysical properties are based on empirical Gaussian distributions that can be further customized to fit observed data. In addition, a detailed net-to-gross ratio is produced for each modelled case.

11.2 AVO attributes

To test our method we use the porosity and net-to-gross synthetic logs computed in SBED model with sedimentation conditions based on the turbidite system from the Glitne Field. In Figure 25, we show these plots for 80 m thickness of reservoir. First, we consider the homogeneous fluid saturation in reservoir. The anisotropy parameters logs are computed by using available rock physics data. The water saturation results in increase in both anisotropy parameters, but parameter δ remains negative. Water saturation results in amplitude increase in the mid-reservoir section for both central frequencies. The oil-water contact (OWC) scenario (20% water saturation above and 90 percent water saturation below the OWC) results in elastic properties can easily be seen on the upscaled log data. The position for OWC is quite pronounced in elastic properties. The synthetic near- and far-offset traces results in more smooth reflection in the mid-reservoir section. The advantages of proposed

technology are following: 1) the sedimentology scenario, 2) the fluid saturation scenario, 3) the AVO attributes from ultra-thin layered reservoirs taking into account the interbedded multiples.

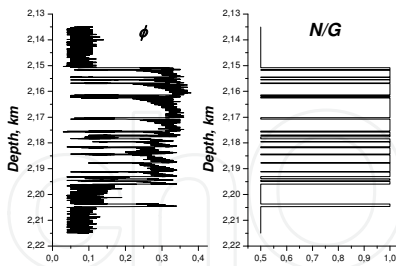


Fig. 25. The porosity (to the left) and net-to-gross (to the right) vertical profiles generated by SBED for the reservoir zone (Stovas et al., 2007).

12. Conclusions

In this chapter we discuss different issues related to wave propagation in layered media with major focus on finely (thin) layered media. We widely use the matrix propagator technique and discuss very important symmetries of propagator and reflection/transmission matrices. The weak-contrast reflection and transmission coefficients are derived in first- and second-order approximations. The periodically layered medium is a fundamental example to illustrate the effect of periodicity on the wavefield, and we use this example to derive reflection and transmission responses. We analyze the caustics of the shear waves in a single layer and in multilayered media. Few seismic applications mostly related to seismic upscaling problem are discussed at the end of this chapter.

13. Acknowledgments

Alexey Stovas acknowledges the ROSE project at NTNU for financial support. Yury Roganov acknowledges Tesseral Technologies Inc. for financial support.

14. References

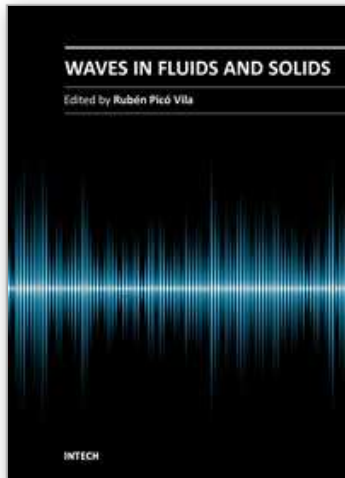
- Aki, K. & Richards, P. (1980). *Quantitative seismology. Theory and methods*, W.H. Freeman and Company, San Francisco, ISBN 9781891389634.
- Backus, G.E. (1962). Long-wave elastic anisotropy produced by horizontal layering. *J.Geophys.Res.*, Vol.67, pp. 4427-4440, ISSN 0148-0227.
- Bamberger, A.; Chavent, G.; Hemon, Ch. & Lailly, P. (1982). Inversion of normal incidence seismograms. *Geophysics*, Vol.47, pp. 757-770, ISSN 0016-8033.
- Banik, N.C.; Lerche, I. & Shuey, R.T. (1985a). Stratigraphic filtering, Part I: Derivation of the O'Doherty-Anstey formula. *Geophysics*, Vol.50, pp. 2768-2774, ISSN 0016-8033.
- Banik, N.C.; Lerche, I.; Resnik, J.R. & Shuey, R.T. (1985b). Stratigraphic filtering, Part II: Model spectra. *Geophysics*, Vol.50, pp. 2775-2783, ISSN 0016-8033.
- Braga, A.M. & Herrmann G. (1992). Floquet waves in anisotropic periodically layered composites. *J. Acoust. Soc. Am.*, Vol.91, pp. 1211-1227, ISSN 0001-4966.
- Brekhovskikh, L.M. (1960). *Waves in layered media*, Academic Press, Applied Mathematics and Mechanics, Vol.6, New York.

- Carcione, J.M.; Kosloff, D. & Behle, A. (1991). Long-wave anisotropy in stratified media: A numerical test. *Geophysics*, Vol.56, pp. 245-254, ISSN 0016-8033.
- Carcione, J.M. (2007). *Wavefields in real media: Wave propagation in anisotropic, anelastic and porous media* (second edition), Elsevier, ISBN 0950-1401, Amsterdam-London-Paris.
- Chapman, C.H. (1994). Reflection/transmission coefficients reciprocities in anisotropic media. *Geophysical Journal International*, Vol.116, pp. 498-501, ISSN 0956-540X.
- Cvetich, M. & Picman, L. (1981). Scattering states for a finite chain in one dimension. *J.Phys.A.*, Vol.14, pp. 379-382, ISSN 0305-4470.
- Dellinger, J.A. (1991). Anisotropic seismic wave propagation. PhD Thesis, Stanford, CA, USA (<http://sepwww.stanford.edu/theses/sep69/>).
- Fryer G. J. & Frazer L. N. (1987). Seismic waves in stratified anisotropic media-II. Elastodynamic eigensolutions for some anisotropic systems. *Geophys. J. R. astr. Soc.*, Vol.91, pp. 73-101, ISSN 0305-8719.
- Gassmann, F. (1951). Uber die Elastitat poroser Medien, *Vier. Der Natur. Gesellschaft in Zurich*, Vol.96, pp. 1-23.
- Gelinsky, S. & Shapiro, S.A. (1997). Poroelastic Backus averaging for anisotropic layered fluid- and gas-saturated Sediments. *Geophysics*, Vol.62, pp. 1867-1878, ISSN 0016-8033.
- Gradshteyn, I.S. & Ryzhik, I.M. (1995). *Tables of integrals, series and products* (seventh edition), ISBN 0-12-059876-0, Academic Press.
- Griffiths, D.J. & Steinke, C.A. (2001). Waves in locally periodic media. *Am.J.Phys.*, Vol.69, pp. 137-154, ISSN 0096-0322.
- Haskell, N.A. (1953). The dispersion of surface waves in multilayered media. *Bulletin of the Seismological Society of America*, Vol.43, pp. 17-34, ISSN 0037-1106.
- Helbig, K. (1984). Anisotropy and dispersion in periodically layered media. *Geophysics*, Vol.49, pp. 364-373, ISSN 0016-8033.
- Hovem, J.M. (1995). Acoustic waves in finely layered media. *Geophysics*, Vol.60, pp. 1217-1221, ISSN 0016-8033.
- Kennett, B.L.N. (1983). *Seismic wave propagation in stratified media*. Cambridge University Press.
- Marion, D. & Coudin, P. (1992) From ray to effective medium theories in stratified media: An experimental study, *Expanded Abstract of 62nd Ann.Internat.Mtg., Soc.Expl.Geophys.*, pp. 1341-1343, New Orleans, USA.
- Marion, D.; Mukerji, T. & Mavko, G. (1994). Scale effects on velocity dispersion: From ray to effective theories in stratified media. *Geophysics*, Vol.59, pp. 1613-1619, ISSN 0016-8033.
- Morlet, J.; Atens, G.; Fourgeau, E., & Giard, D. (1982a). Wave propagation and sampling theory - Part I: Complex signal and scattering in multilayered media. *Geophysics*, Vol.47, pp. 203-221, ISSN 0016-8033.
- Musgrave M.J.P. (1970). *Crystal Acoustics*. San Francisco: Holden - Day.
- Nordahl, K.; Ringrose, P.S. & Wen, R. (2005). Petrophysical characterization of a heterolithic tidal reservoir interval using a process-based modeling tool. *Petroleum Geoscience* Vol.11, pp. 17-28.
- O'Doherty, R.F. & Anstey, N.A. (1971). Reflections on amplitudes. *Geophys. Prospect.*, Vol.19, pp. 430-458, ISSN 0016-8025.

- Peano, G. (1888). Intégration par séries des équations différentielles linéaires. *Math. Ann.* Vol.32, pp. 450–456.
- Pease, M.C. (1965). *Methods of Matrix Algebra*, Academic Press, New York.
- Peyton, R.G. (1983). *Elastic wave propagation in transversely isotropic media*, Martinus Nijhoff Publishers, The Netherlands.
- Roganov, Y. & Roganov, V. (2008). Dispersion of low-frequency waves in periodically layered media. *Geophysical Journal* Vol.30, pp. 27-33, ISSN 0203-3100 (in Russian).
- Roganov, Yu. (2008). Caustics on the wave fronts in transversely isotropic media. *Geoinformatika* N3, 29-34, ISSN 1684-2189 (in Russian).
- Roganov, Yu. & Stovas, A. (2010). On shear wave triplications in a multi-layered VTI medium. *Geophysical Prospecting*, Vol.58, N4, pp. 549-559, ISSN 0016-8025.
- Roganov, Yu. & Stovas, A. (2011). Caustics in a periodically layered transversely isotropic medium with vertical symmetry Axis. *Geophysical Prospecting*, (accepted, early view), ISSN 0016-8025.
- Schoenberger, M. & Levin, F.K. (1974). Apparent attenuation due to intrabed multiples. *Geophysics*, Vol.39, pp. 278-291, ISSN 0016-8033.
- Schoenberg, M. & Daley T.M. (2003). qSV wavefront triplication in transversely isotropic material. *Expanded Abstracts of 73th Annual International Meeting, SEG*, pp. 137-140, Dallas, USA, October 26-31.
- Schoenberg, M. & Helbig K. (1997). Orthorhombic media: Modeling elastic wave behavior in vertically fractured earth. *Geophysics*, Vol.62, pp. 1954–1974, ISSN 0016-8033.
- Shapiro, S.A.; Hubral, P. & Ursin, B. (1996). Reflectivity/transmissivity for one dimensional inhomogeneous random elastic media: dynamic-equivalent medium approach. *Geoph. J. Int.*, Vol.126, pp. 184-196, ISSN 0956-540X.
- Shapiro, S.A. & Treitel, S. (1997). Multiple scattering of seismic waves in multilayered structures. *Physics of the Earth and Planetary Interiors*, Vol.104, pp. 147-159.
- Stovas, A. & Ursin, B. (2001). Second-order approximations of the reflection and transmission coefficients between two visco-elastic isotropic media. *Journal of Seismic Exploration*, Vol.9, pp. 223-233, ISSN: 0963-0651.
- Stovas, A. & Ursin, B. (2003). Reflection and transmission responses of a layered transversely isotropic viscoelastic medium. *Geophysical Prospecting*, Vol.51, No.5, pp. 447-477, ISSN 0016-8025.
- Stovas, A. & Landrø, M. (2004). Optimal use of PP and PS time-lapse stacks for fluid-pressure discrimination. *Geophysical Prospecting*. Vol.52, pp. 1-12, ISSN 0016-8025.
- Stovas, A. & Arntsen, B. (2006). Vertical propagation of low frequency waves in finely layered medium. *Geophysics*, Vol.71, N3, pp. T87-T94, ISSN 0016-8033.
- Stovas, A.; Landrø, M. & Avseth, P. (2006). AVO attribute inversion for finely layered reservoirs. *Geophysics*, Vol.71, N3, pp. C25-C36, ISSN 0016-8033.
- Stovas, A. (2007). Phase velocity approximation in a finely layered sediments. *Geophysics*, Vol.72, N5, pp. T57-T59, ISSN 0016-8033.
- Stovas, A. & Ursin, B. (2007). Equivalent time-average and effective medium for periodic layers, *Geophysical Prospecting*, Vol.55, N6, pp. 871-882, ISSN 0016-8025.
- Stovas, A.; Landro, M. & Janbu, M. (2007). Seismic attributes from ultra-thin layered reservoirs. *Oil and Gas*, Vol.62, N2, pp. 147-154.
- Stovas, A. (2009). Power-gradient velocity model. *Geophysics*, Vol.74, No.5, pp. U13-U33, ISSN 0016-8033.

- Stovas, A. & Roganov, Yu. (2009). Slowness surface approximations for qSV-waves in transversely isotropic media. *Geophysical Prospecting*, Vol. 57, pp. 1-11, ISSN 0016-8025.
- Thomson, W.T. (1950). Transmission of elastic waves through a stratified solid. *J. Appl. Phys.* Vol. 21, pp. 89-93, ISSN 0021-8979.
- Thomsen, L. (1986). Weak elastic anisotropy. *Geophysics*, Vol.51, pp. 1954-1966, ISSN 0016-8033.
- Thomsen, L. & Dellinger, J. (2003). On shear-wave triplication in transversely isotropic media. *Journal of Applied Geophysics*, Vol.54, pp. 289 – 296, ISSN: 0926-9851.
- Tsvankin, I. (1995). Seismic wavefields in layered isotropic media, Samizdat Press, Golden, USA.
- Tygel, M.; Ursin, B. & Stovas, A. (2007). Convergence of the traveltime power series for a layered transversely isotropic medium. *Geophysics*, Vol. 72, No.2, pp. D21-D28, ISSN 0016-8033.
- Ursin, B. (1983). Review of elastic and electromagnetic wave propagation in horizontally layered media. *Geophysics*, Vol.48, No.8, pp.1063-1081, ISSN 0016-8033.
- Ursin, B. (1987). The plane-wave reflection and transmission response of a vertically inhomogeneous acoustic medium. In Bernabini, M.; Carrion, P.; Jacovitti, G.; Rocca, F.; Treitel, S. & Worthington, M., eds., *Deconvolution and inversion*, pp. 189-207, Blackwell Sc. Publ., Oxford, ISBN: 9780632019014.
- Ursin, B. & Haugen, G.U. (1996). Weak-contrast approximation of the elastic scattering matrix in anisotropic media. *Pure and Applied Geophysics*, Vol.148, pp. 685- 714, ISSN 0033-4553.
- Ursin, B. & Stovas, A. (2002). Reflection and transmission responses of a layered isotropic visco-elastic medium. *Geophysics* Vol.67, pp. 307-323, ISSN 0016-8033.
- Vavrycuk, V. (2003). Generation of triplication on transversely isotropic media. *Physical Review B*. Vol.68, 054107, ISSN 1098-0121.
- Wen, R. (2004). 3D modeling of stratigraphic heterogeneity in channelized reservoirs: methods and applications in seismic attribute facies classification. *CSEG Recorder*, Vol.29, pp. 38-45.
- Wu, H.; Sprung, D.W.L. & Martorell, J. (1993). Periodic quantum wires and their quasi-one-dimensional nature. *J.Phys.D*, Vol.26, pp. 798-803, ISSN 0022-3727.

IntechOpen



Waves in Fluids and Solids

Edited by Prof. Ruben Pico Vila

ISBN 978-953-307-285-2

Hard cover, 314 pages

Publisher InTech

Published online 22, September, 2011

Published in print edition September, 2011

Acoustics is a discipline that deals with many types of fields wave phenomena. Originally the field of Acoustics was consecrated to the sound, that is, the study of small pressure waves in air detected by the human ear. The scope of this field of physics has been extended to higher and lower frequencies and to higher intensity levels. Moreover, structural vibrations are also included in acoustics as a wave phenomena produced by elastic waves. This book is focused on acoustic waves in fluid media and elastic perturbations in heterogeneous media. Many different systems are analyzed in this book like layered media, solitons, piezoelectric substrates, crystalline systems, granular materials, interface waves, phononic crystals, acoustic levitation and soft media. Numerical methods are also presented as a fourth-order Runge-Kutta method and an inverse scattering method.

How to reference

In order to correctly reference this scholarly work, feel free to copy and paste the following:

Alexey Stovas and Yury Roganov (2011). Acoustic Waves in Layered Media - From Theory to Seismic Applications, Waves in Fluids and Solids, Prof. Ruben Pico Vila (Ed.), ISBN: 978-953-307-285-2, InTech, Available from: <http://www.intechopen.com/books/waves-in-fluids-and-solids/acoustic-waves-in-layered-media-from-theory-to-seismic-applications>

INTECH
open science | open minds

InTech Europe

University Campus STeP Ri
Slavka Krautzeka 83/A
51000 Rijeka, Croatia
Phone: +385 (51) 770 447
Fax: +385 (51) 686 166
www.intechopen.com

InTech China

Unit 405, Office Block, Hotel Equatorial Shanghai
No.65, Yan An Road (West), Shanghai, 200040, China
中国上海市延安西路65号上海国际贵都大饭店办公楼405单元
Phone: +86-21-62489820
Fax: +86-21-62489821

© 2011 The Author(s). Licensee IntechOpen. This chapter is distributed under the terms of the [Creative Commons Attribution-NonCommercial-ShareAlike-3.0 License](#), which permits use, distribution and reproduction for non-commercial purposes, provided the original is properly cited and derivative works building on this content are distributed under the same license.

IntechOpen

IntechOpen